

INFORMATION TO USERS

This reproduction was made from a copy of a document sent to us for microfilming. While the most advanced technology has been used to photograph and reproduce this document, the quality of the reproduction is heavily dependent upon the quality of the material submitted.

The following explanation of techniques is provided to help clarify markings or notations which may appear on this reproduction.

1. The sign or "target" for pages apparently lacking from the document photographed is "Missing Page(s)". If it was possible to obtain the missing page(s) or section, they are spliced into the film along with adjacent pages. This may have necessitated cutting through an image and duplicating adjacent pages to assure complete continuity.
2. When an image on the film is obliterated with a round black mark, it is an indication of either blurred copy because of movement during exposure, duplicate copy, or copyrighted materials that should not have been filmed. For blurred pages, a good image of the page can be found in the adjacent frame. If copyrighted materials were deleted, a target note will appear listing the pages in the adjacent frame.
3. When a map, drawing or chart, etc., is part of the material being photographed, a definite method of "sectioning" the material has been followed. It is customary to begin filming at the upper left hand corner of a large sheet and to continue from left to right in equal sections with small overlaps. If necessary, sectioning is continued again—beginning below the first row and continuing on until complete.
4. For illustrations that cannot be satisfactorily reproduced by xerographic means, photographic prints can be purchased at additional cost and inserted into your xerographic copy. These prints are available upon request from the Dissertations Customer Services Department.
5. Some pages in any document may have indistinct print. In all cases the best available copy has been filmed.

**University
Microfilms
International**
300 N. Zeeb Road
Ann Arbor, MI 48106

1319840

MARSHALL, ROGER ALLEN

A SPECTROPHOTOMETRIC STUDY OF THE NITROGEN(DOUBLET-D) AND
NITROGEN(DOUBLET-P) STATES IN THE AURORA

UNIVERSITY OF ALASKA

M.S. 1982

**University
Microfilms
International** 300 N. Zeeb Road, Ann Arbor, MI 48106

A SPECTROPHOTOMETRIC STUDY OF THE
NI[²D] AND NI[²P] STATES IN THE AURORA

A
THESIS

Presented to the Faculty of the University of Alaska
in Partial Fulfillment of the Requirements
for the Degree of

MASTER OF SCIENCE

By
Roger Allen Marshall, A.A.S., B.S.

Fairbanks, Alaska

May 1982

A SPECTROPHOTOMETRIC STUDY OF THE
NI[²D] AND NI[²P] STATES IN THE AURORA

RECOMMENDED:

Thomas P. Hallinan

Samuel A. Lopez

John Murray

Charles J. Decker

Alvin J. Rinzee

Chairman, Advisory Committee

Alvin J. Rinzee

Head, Space Physics and Atmospheric
Sciences Program

APPROVED:

K. B. Coakley
Vice Chancellor for Research and Advanced Study

Feb. 26, 1982
Date

ABSTRACT

The optical emissions from two excited states of atomic nitrogen were observed in the aurora in order to determine the relationship between their absolute intensities when excited by particles of varied energies. In order to accomplish this, auroral emissions at 5200 Å and 3466 Å originating from the $\text{NI}[^2\text{D} \rightarrow ^4\text{S}]$ and $\text{NI}[^2\text{P} \rightarrow ^4\text{S}]$ transitions were observed simultaneously using two co-aligned Ebert-Fastie spectrometers from Longyearbyen, Svalbard. The relationship was determined to be linear with the ratio of 5200 Å to 3466 Å intensities being 1.84 ± 0.40 . This value differs significantly from current theoretical prediction ($I(5200 \text{ Å})/I(3466 \text{ Å}) \approx 30$) suggesting that the reaction of N_2 with O to form the $\text{NI}[^2\text{D}]$ state may not be as efficient as previously assumed or that another source of $\text{NI}[^2\text{P}]$ must be included in the model calculations.

TABLE OF CONTENTS

	Page
ABSTRACT	iii
TABLE OF CONTENTS	iv
LIST OF ILLUSTRATIONS	vi
LIST OF TABLES	viii
ACKNOWLEDGEMENTS	ix
CHAPTER 1 INTRODUCTION	1
CHAPTER 2 INSTRUMENTATION	10
2.1 The Optical System	10
2.2 The Scanning Spectrophotometers	10
2.3 The Meridian Scanning Photometer	16
2.4 The All-Sky Camera	18
2.5 The Data Processing System	19
CHAPTER 3 OBSERVATIONS AND DATA PREPARATION	26
3.1 The Objective	26
3.2 The Observing Program	26
3.3 Field Calibration Procedures	29
3.4 Absolute Intensity Calibration	30
3.5 Atmospheric Extinction	36
3.6 Data Analysis	37
CHAPTER 4 ATOMIC NITROGEN IN THE AURORA	46
4.1 Modeling the Excited States of Atomic Nitrogen	46
4.2 Atomic Nitrogen in the Auroral Atmosphere	47

	Page
4.3 Theoretical Considerations	52
4.4 Model Calculations	54
CHAPTER 5 SUMMARY	60
APPENDIX ERROR CALCULATIONS	62
BIBLIOGRAPHY	65

LIST OF ILLUSTRATIONS

FIGURE		PAGE
1.1	Energy level diagram for the lowest three energy states of atomic nitrogen and the emissions due to transitions between these levels.	3
2.1	Diagram of the Ebert-Fastie scanning spectrophotometer.	12
2.2	The geometry of the grating optics in the Ebert-Fastie spectrometer.	14
2.3	Diagram of the meridian scanning photometer setup.	17
2.4	Block diagram of the data collection system used in the study.	20
2.5	Example of the half-meter spectrometer display. The 5200 Å emission is shown along with pertinent data relating to it.	22
2.6	Example of the 3466 Å one-meter spectrometer emission is displayed with pertinent information related to it.	23
2.7	Example of the 6300 Å meridian scanning photometer emission displayed along with related information.	24
3.1	A plot of the raw 5200 Å versus 3466 Å data. The slope of the best fitting line is 1.62 and the line intersects the 5200 Å axis at 4.3 R.	41

FIGURE		PAGE
3.2	A plot of the reduced 5200 Å versus 3366 Å data. The slope of the best fitting line is 1.84 and the line intersects the 5200 Å axis at -0.2 R.	42
3.3	A plot of the 6300 Å versus 4278 Å data points, made in order to estimate the range of character- istic energies in the auroras observed.	44
A.1	A diagram of the geometry of the absolute intensity calibration setup.	63

LIST OF TABLES

TABLE		PAGE
4.1	The major production and loss mechanisms of the $\text{NI}[^2\text{D}]$ state which produces the 5200 Å emission.	50
4.2	The major production and loss mechanisms for the $\text{NI}[^2\text{P}]$ state which produces the 3466 Å emission.	51

ACKNOWLEDGEMENTS

I would like to thank the entire staff of the Geophysical Institute at the University of Alaska; in particular Gulamabas G. Sivjee, Charles S. Deehr and Gerald J. Romick whose insight and support helped to make this thesis a reality. Also I would like to thank the Norwegian government, the researchers of the University of Oslo and the researchers at the University of Tromsø for their hospitality and support during my visit to Norway.

This research was supported by National Science Foundation grants ATM 77-24837 and ATM 80-12719.

CHAPTER 1

INTRODUCTION

Just two elements, nitrogen and oxygen, compose over 99 percent of the earth's atmospheric volume. Of this, 78 percent is nitrogen, almost all of which exists in the diatomic molecular form, N_2 . In the upper atmosphere diatomic oxygen, O_2 , is dissociated by sunlight to form atomic oxygen, O , the predominant form of oxygen above 200 kilometers (km). More energy is required to photodissociate N_2 than O_2 and relatively little atomic nitrogen, N , is normally present, even at 500 km. At high latitudes the atmosphere is bombarded by energetic particles, principally electrons and protons, forming regions of frequent atmospheric disturbance called auroral ovals. These particles are responsible for producing the Aurora Borealis and the Aurora Australis. The particles may penetrate down to heights of 80 km before being thermalized and nearly 50 percent of the precipitating particle energy is expended in the ionization, dissociation or dissociative ionization of N_2 . These three processes eventually lead to the production of atomic nitrogen (Hyman et al, 1976). Some of these nitrogen atoms are produced in excited states and react much faster with other atmospheric constituents than ground state nitrogen atoms. In this way, an auroral event may significantly affect the chemistry of the upper atmosphere.

In auroras atomic nitrogen may be formed in any of the available electronic states, such as the $4S^0$, $2D^0$, or $2P^0$ states. The excess

electronic energy of excited atomic nitrogen atoms effectively speeds up the interaction of the metastable species with other atmospheric constituents. These reactions may proceed at rates that are orders of magnitude faster than for NI in the ground state. For example, it has been observed that the NI[2D] state reacts much faster than the NI(4S) ground state with O_2 to form nitric oxide, NO (Slanger et al, 1971). Calculations of NO production are therefore very sensitive to the relative abundances of these two states (Hyman et al, 1976; Rees and Roble, 1979). Reports of anomalous NO concentrations in auroras (Zipf et al, 1970; Donahue, 1972; Swinder and Narcisi, 1974) have promoted the need for a quantitative measure of the production rate of the excited states of atomic nitrogen through the emissions which are their signatures.

The absolute abundances of atomic nitrogen in its various excited states are obtained by observing the optical emissions from the excited states. Atomic nitrogen produced by the interaction of energetic auroral electrons with atmospheric N_2 , is formed primarily in the lowest electronic energy states, i.e. in the 4S , 2D and 2P levels. Atomic nitrogen formed in the 2P states can make transitions to either the 4S or the 2D states (see Figure 1.1). The $^2P_{1/2,3/2} \rightarrow ^2D_{3/2,5/2}$ transitions produce two closely spaced doublet emissions at wavelengths of 10,395 and 10404 Angstroms (\AA) while the $^2P_{1/2} \rightarrow ^4S_{3/2}$ transitions lead to one closely spaced doublet at 3466.4 \AA . The auroral intensities of these emissions depend on the total number of NI[2P] atoms formed in the aurora. The $^2D_{3/2,5/2} \rightarrow ^4S_{3/2}$ transitions produce a more widely spaced doublet with wavelengths of 5198.5 \AA and 5200.7 \AA .

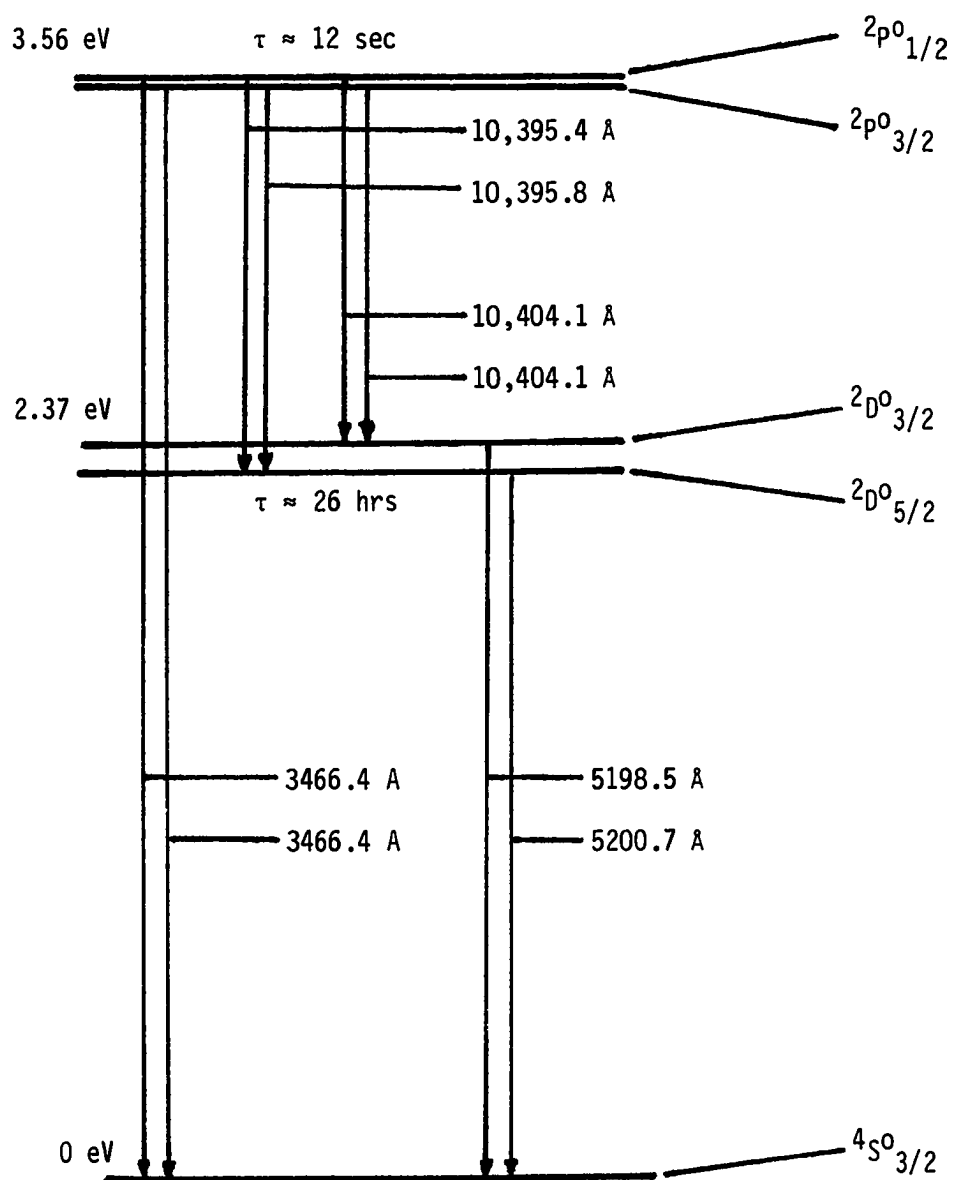


Figure 1.1 Energy level diagram of the atomic nitrogen $4S^0$ ground state and the $2D^0$ and $2P^0$ excited electronic states.

Although studies have been done where these two emissions are considered as separate entities (Sivjee et al, 1981) most observations of these lines have used equipment with insufficient resolution to separate them. These two emissions will be collectively referred to as the 5200 Å doublet, except where it is necessary to be more explicit. The ratio of 5200 Å to 3466 Å is indicative of the relative populations of $\text{NI}[^2\text{D}]$ and $\text{NI}[^2\text{P}]$ in auroras. This study is primarily concerned with the determination of this ratio through simultaneous spectrophotometric observations of the auroral 5200 Å and 3466 Å emissions. Both of these NI doublet emissions are relatively weak in the aurora, their intensities ranging from a few rayleighs (R) during aurorally quiet conditions, to a few hundred rayleighs during aurorally disturbed conditions.

The 5200 Å doublet was first observed in the aurora by Slipher and Sommer (1929). Being a weak emission, it was not observed in the airglow until twenty years later by Courtes (1950). The 3466 Å line was also first observed in the aurora, by Kaplan (1938). Both the $[^2\text{P} \rightarrow ^4\text{S}]$ and $[^2\text{D} \rightarrow ^4\text{S}]$ transitions are "forbidden" by the spin change rule since both must change multiplicities. The $[^2\text{D} \rightarrow ^4\text{S}]$ transition is doubly forbidden since it also breaks the electric dipole selection rule for orbital angular momentum, i.e. $\Delta l = \pm 1$. These levels are called metastable and radiate according to electric quadrupole and magnetic dipole processes. The radiative lifetime of metastable levels is usually greater than 10^{-6} seconds. The Einstein transition probabilities $A(i,j)$, are inversely proportional to the radiative

lifetimes. For the 5200 Å and 3466 Å emissions the A values were first calculated theoretically by Pasternak (1940). Some of these values were modified slightly several years later to account for interactions between electron orbital shells (Garstang, 1952, 1956). An effective Einstein A coefficient for the [$2P \rightarrow 4S$] doublet transition was determined to be 5.4×10^{-3} per second. This value is considered accurate within 20 percent (Garstang, 1956). The calculated radiative lifetime of the NI[$2P$] state (τ) is about 12 seconds. The [$2D \rightarrow 4S$] transition has an effective A coefficient of $1.06 \pm 0.5 \times 10^{-5}$ per second (Garstang, 1956). The radiative lifetime of the NI[$2D$] state is approximately 26 hours.

Not all excited atoms are de-excited radiatively. When in metastable states, most atoms suffer collisions with ambient particles and lose their excess energy. During this process, called quenching, energy may be lost by exciting the quenching species or it may be transformed into the energy of motion by altering the velocity of both particles. At auroral heights the [NI] 5200 Å radiation has an effective lifetime similar to the [OI] 6300 Å emission and its intensity appears to vary much like the [OI] 6300 Å radiation (Torr et al, 1976). This is apparently due to the effect of quenching by atomic oxygen resulting in the formation of NO. The importance of the NI[$2D$] state in the formation of nitric oxide has led to many studies of the 5200 Å emission (Torr et al, 1976; Frederick and Rusch, 1977; Rusch and Gerard, 1980; Sivjee et al, 1981). Studies of the NI[$2P$] state are more rare and most have been done only recently (Vallance Jones

and Gattinger, 1975; Young and Dunn, 1975; Gerard and Harang, 1980). Only recently has a determination of the proportional yield of N^+ , $NI[{}^2P]$, $NI[{}^2D]$ and $NI(4S)$ atoms due to electron impact dissociation been accomplished (Zipf et al, 1980). The long radiative lifetimes of the 3466 Å and 5200 Å emissions makes their study a formidable task. A laboratory study is almost impossible because of the large probability of collisional deactivation with other atoms or the walls of the vacuum chamber. As a result the radiation that is emitted is very weak producing a signal that is usually indistinguishable from the background noise. On the other hand, in the atmosphere above 120 km, the density of the air is small and thus the collision frequency is low enough to allow a significant proportion of excited nitrogen atoms to radiate.

Artificial means of exciting atmospheric emissions have been attempted with limited success (Hess et al, 1971; Davis et al, 1971; Davis et al, 1980). Such methods have the advantage of exciting the metastable species in a limited atmospheric region where physical and chemical conditions are relatively uniform. Still, problems involving optical tracking of such a weak signal and the cost of a rocket launch prevent this technique from being used routinely. The advent of regular space shuttle missions may make this type of study more common in the future. The aurora supplies a means of exciting the $NI[{}^2D]$ and $NI[{}^2P]$ states through, primarily, electron bombardment. Most of the 5200 Å and 3466 Å emission is thought to be produced between the heights of 140 km and 300 km so it is important to look at auroras

which occur in this region. Electrons precipitating into the atmosphere during most auroral events have almost a continuous distribution of energies, from thermal to relativistic. The differential energy spectrum of this electron flux is usually represented by one of several functional distributions such as Gaussian, exponential, or Maxwellian. The functional energy dependence varies from one aurora to another as well as in auroras formed at different local times. On the nightside of the oval the typical aurora results from particles having characteristic energies of 2 to 10 thousand electron volts (KeV). These particles dissipate most of their energy at altitudes between 110 km and 130 km. At these altitudes quenching of $\text{NI}[^2\text{P}]$ and $\text{NI}[^2\text{D}]$ is dominant, hence very little 3466 Å and 5200 Å emissions are produced. These high energy electrons also excite other more intense molecular band emissions which tend to mask out weak lines like 5200 Å and 3466 Å. On the day side of the auroral oval, the precipitating electrons have a different energy spectrum, frequently having characteristic energies of less than 1 KeV. The lower energy electrons lose most of their energy to the atmosphere between 140 km and 500 km, where metastable levels live long enough to radiate because of lower collision frequencies. An observing site permitting both day and night-time measurements would have the distinct advantage of being able to observe electron-atom collision processes over a wide range of energies in an almost thermally collisionless reaction chamber, having no walls.

A group of islands in the North Atlantic, collectively known as Svalbard, provide an excellent location for the study of both day and

night-time auroras. Svalbard's geographic location at 80 degree north latitude is far enough poleward to allow 24 hour observation of the aurora for over 2 months of the year around the winter solstice. Its invariant geomagnetic latitude of 75 degrees north permits observations of the magnetospheric cusp under both quiet and moderately disturbed conditions. For these reasons a ground-based optical observing facility was established in Longyearbyen, Svalbard (Geographic latitude; 78.2 degrees north and longitude; 11.9 degrees east), in the winter of 1978 as part of the International Magnetospheric Study (IMS) program. This was begun as a multi-national auroral expedition which is scheduled to continue through 1983. It is manned by researchers from the Universities of Tromsø and Oslo (Norway), the University of Alaska (United States), Ulster Polytechnic (United Kingdom) and the University of Saskatchewan (Canada). During the months of December and January the solar depression angle in Longyearbyen is never less than 6 degrees and for most of the period it is more than 9 degrees. Degradation of auroral optical signal due to scattered sunlight is therefore minimal, a definite advantage when dealing with weak auroral emissions.

The most obvious characteristic of the aurora is its temporal and spatial variability. This requires intensity measurements to be made more quickly than any gross changes occurring in the aurora if the data are to be meaningful. For rapid measurements of weak emissions, large throughput optical radiation detection equipment is necessary. The Geophysical Institute of the University of Alaska has developed a

highly sensitive electro-optical system consisting of two co-aligned, large throughput, Ebert-Fastie scanning spectrophotometers and a four channel, fixed bandpass, meridian scanning photometer (MSP), operating in the photon counting mode. These instruments are interfaced to an interactive digital data processing and storage system, which is capable of data collection and storage while at the same time permitting real time analysis. The data used in this study were taken utilizing this system as part of the Svalbard Multi-National Auroral Expedition in Longyearbyen, during the 1979-1980 observing season. Absolute intensity measurements of [NI] 3466 Å and 5200 Å emissions in various day and night-time auroras (excited by electrons with average energies differing by almost an order of magnitude) and their analysis in terms of the relative populations of NI[²D] and NI[²P] states is the principle concern of this thesis.

Chapter 2 describes the experimental facilities employed for the study. Results of the observational program are presented in Chapter 3 and their analysis will be discussed in Chapter 4.

CHAPTER 2

INSTRUMENTATION

2.1 The Optical System

The electro-optical system employed for the studies of NI[²P] and NI[²D] in auroras consists of two spectrometers and several photometers all operating in the photon counting mode and coupled to a digital, real-time, electronic operating system. In addition, an all-sky camera provided a continuous record of auroral activities and the extent of any cloud cover. In this chapter the operational principles and physical descriptions of the data acquisition systems are presented.

The instruments may be divided into three parts; light gathering and dispersion optics, detectors for converting the optical radiation to electrical pulses and the recording and analysis of the digitally coded information about the auroral emissions. Descriptions of the first two segments involving the optics and detectors are presented in sections 2.1, 2.2, 2.3, and 2.4. The last section of this chapter describes the digital electronic system used for data gathering, recording and analysis.

2.2 The Scanning Spectrophotometers

The heart of the entire optical detection system consists of two co-aligned scanning spectrophotometers operating in the photon counting mode and mounted inside an insulated, heated and steerable container. The container is a modified searchlight housing in which is mounted a one-meter and a one half-meter (focal lengths) Ebert-Fastie spectro-

meter, having identical fields of view (FOV) (approximately 7 degrees square). An insulated plastic dome protects the instruments from the elements and provides a temperature controlled environment. Each spectrometer views the sky through an open hole in the dome which is capped when the instrument is not in use. The searchlight housing is remotely steerable and can be directed to view any part of the sky.

The configuration of the Ebert-Fastie spectrometer is shown in Figure 2.1. The optical system of Ebert uses a spherical mirror to render the incoming light parallel and a plane reflection grating to diffract this parallel beam into its component wavelengths. The inherent astigmatism in design of the Ebert spectrometer was corrected by Fastie (1952) who introduced curved entrance and exit slits. The use of curved slits also corrected an error in wavelength at the exit slit which had previously required the slit to be short. The incident light passes through an order-sorting pre-filter at the entrance slit and reflects off the first half of a 40 cm long section of a spherical mirror, having a 2 m radius of curvature. The slit plate lies in the focal plane of the 40 cm Ebert mirror so the light rays from the entrance slit, reflected from the mirror, are rendered parallel. The light is then reflected from the 25.6 cm x 15.4 cm, 1200 line per mm, plane-grating into component colors. The second half of the Ebert mirror focuses the dispersed light at its focal plane where the exit slit permits a small band of wavelengths to pass through it.

Directly behind the exit slit is a red sensitive E-type photomultiplier tube (PMT) with an extended S-20, corrugated photocathode.

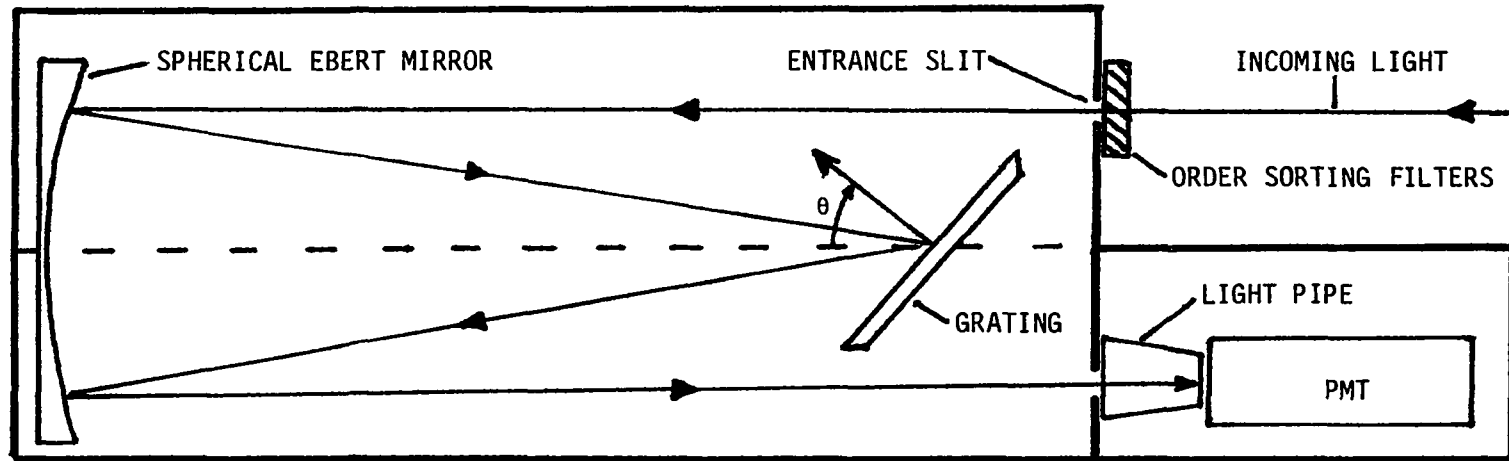


Figure 2.1 The optical arrangement of the Ebert-Fastie scanning spectrometer.

The PMT housed in a thermoelectric cooler which is kept at -25 degrees centigrade to reduce thermal noise. The photomultiplier's signal is fed into a pulse-amplifier-discriminator (PAD) which recognizes only pulses of a set voltage level or greater and then shapes the output pulse to be compatible with the computer's interfacing circuit. The PAD's rejection of low level pulses originating from the dynodes helps to reduce the background noise still further.

The spectrum of the light leaving the spectrometer at the exit slit is centered about a wavelength given by the grating equation:

$$n\lambda = d(\sin i + \sin r) \quad (2-1)$$

Where λ is the wavelength, $n = 0, 1, 2, \dots$, is the order of the grating, d is the spacing between grooves in the grating and i and r are the angles of incident and diffracted beams. As shown in Figure 2.2, $i = \theta - \phi$ and $r = \theta + \phi$. With a bit of manipulation equation 2-1 reduces to

$$n\lambda = 2d \sin \theta \cos \phi \quad (2-2)$$

The term $\cos \phi$ is a fixed value depending only on the dimensions of the instrument. The wavelengths focused on the exit slit are proportional to the sine of the angle θ between the grating normal and symmetry axis of the spectrometer. A linear scan of the wavelengths is produced by rotating the grating using a coupling arm riding on a sine-cam, which is driven by either a stepping or a synchronous motor. A set of 10 cams allows a choice of free spectral ranges between 150 Å and 5700 Å in the first order. Corning glass filters are used to select which order (n in equations 2-1 and 2-2) is passed into the spectrometer. These filters are mounted directly in front of the entrance

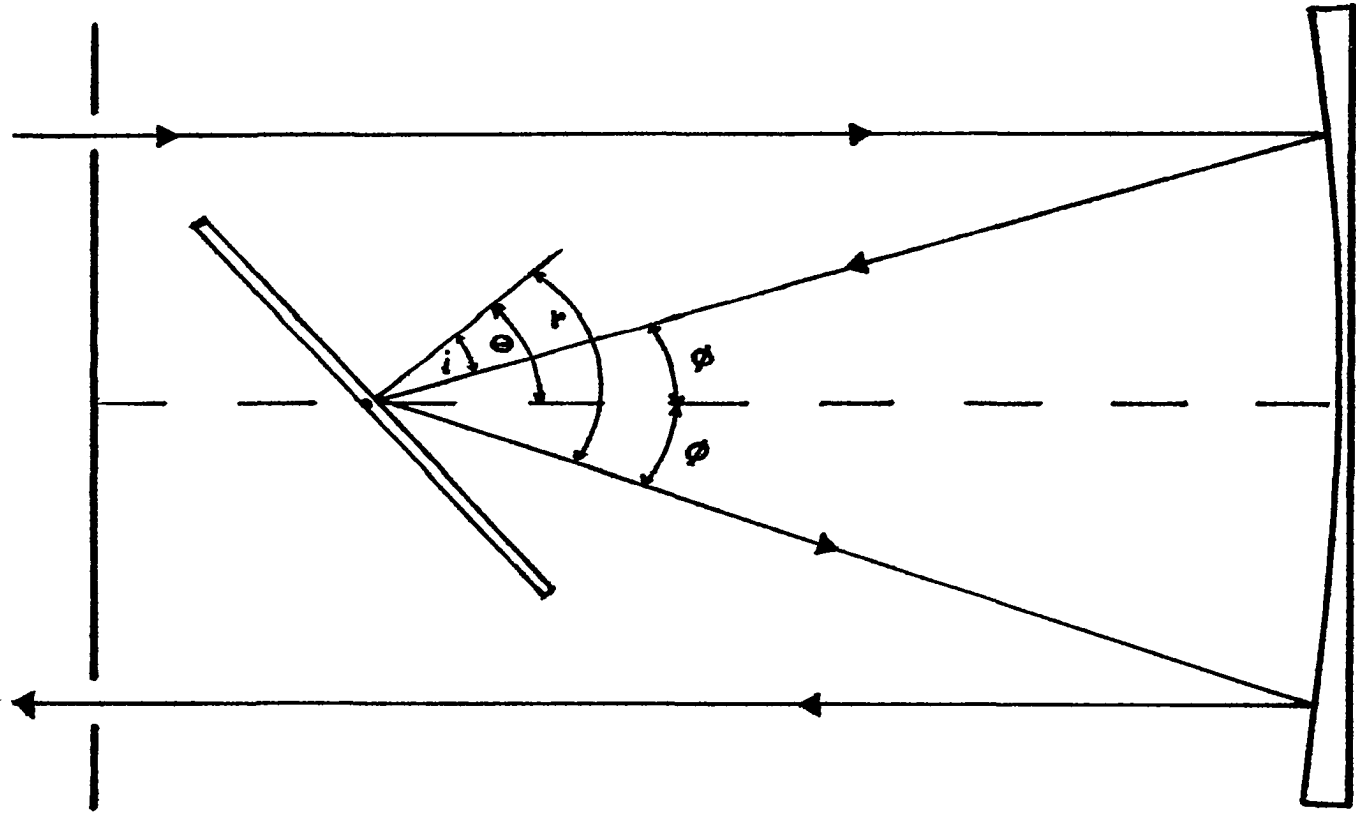


Figure 2.2 The geometry of the grating optics in the Ebert-Fastie spectrometer.

slit. The slit width is varied by a micrometer type adjustment which pushes a wedge into the spring-loaded jaw assembly to open the slit. The slitwidth may be varied from .1 mm to 10 mm as the situation requires.

The output of the spectrometer, in photons, can be shown to be given by:

$$S = BTA_s A_g \cos\theta / F^2 \quad (2-3)$$

where B is the spectral brightness of the source in photons/cm²/ster, T is the transmission, A_s and A_g are the areas of the entrance slit and grating, respectively, and F is the focal length of the instrument. Since the spectrometer's output, S , is proportional to the length of the slit, a large throughput can then be achieved by increasing A_s and A_g (for a given slitwidth). The modification of the Ebert design by Fastie corrected the inherent wavelength error by curving the slits which allowed the slit length to be increased, providing a significant increase in signal strength. Our spectrometer uses the maximum slit length permitted by the grating employed which has 15 cm long ruled grooves.

During airglow and auroral observations of extremely weak optical emissions the spectrometers are rarely used at their highest resolution since it usually becomes necessary to open the slitwidth in order to allow enough light in to provide a sufficiently usable signal. Since the spectrometer's resolution is a function of the slit width, the result is to sacrifice resolution for signal strength. When detecting low-level signals it is often useful to sum several scans in order to

improve the signal-to-noise ratio. If each scan is not accurately initiated, summing successive scans results in a smearing of the signal. This is prevented by initiating the scan with a pulse from an optical pick-up which senses a hole in the cam during the fly-back period. The fly-back occurs as the cam returns the grating back to its initial scan angle.

2.3 The Meridian Scanning Photometer

The meridian scanning photometer (MSP) is positioned to scan the magnetic meridian from north to south. The MSP is housed in a small insulated and heated building which provides protection from inclement weather and temperature fluctuations. The latter is important to ensure a constant bandpass for the interference filters in the photometers. Clear plastic panels in the walls and the roof provide the necessary 180 degree view of the sky for the detectors. The MSP is composed of four fixed bandpass photometers mounted in a close parallel group each viewing a plane mirror positioned at 45 degrees to their optical axis (see Figure 2.3). The mirror is rotated approximately three times a minute allowing each of the photometers to scan the meridian once every revolution of the mirror. The incoming light is reflected from the rotating mirror directly into an interference filter located in the front of each field lens. The interference filters permit a narrow (approximately 15 Å) band of light centered at the wavelength of interest to enter the detector. This study was concerned with only two of the four emissions detected by the photometers, the red auroral emission of atomic oxygen at 6300 Å and the blue emission

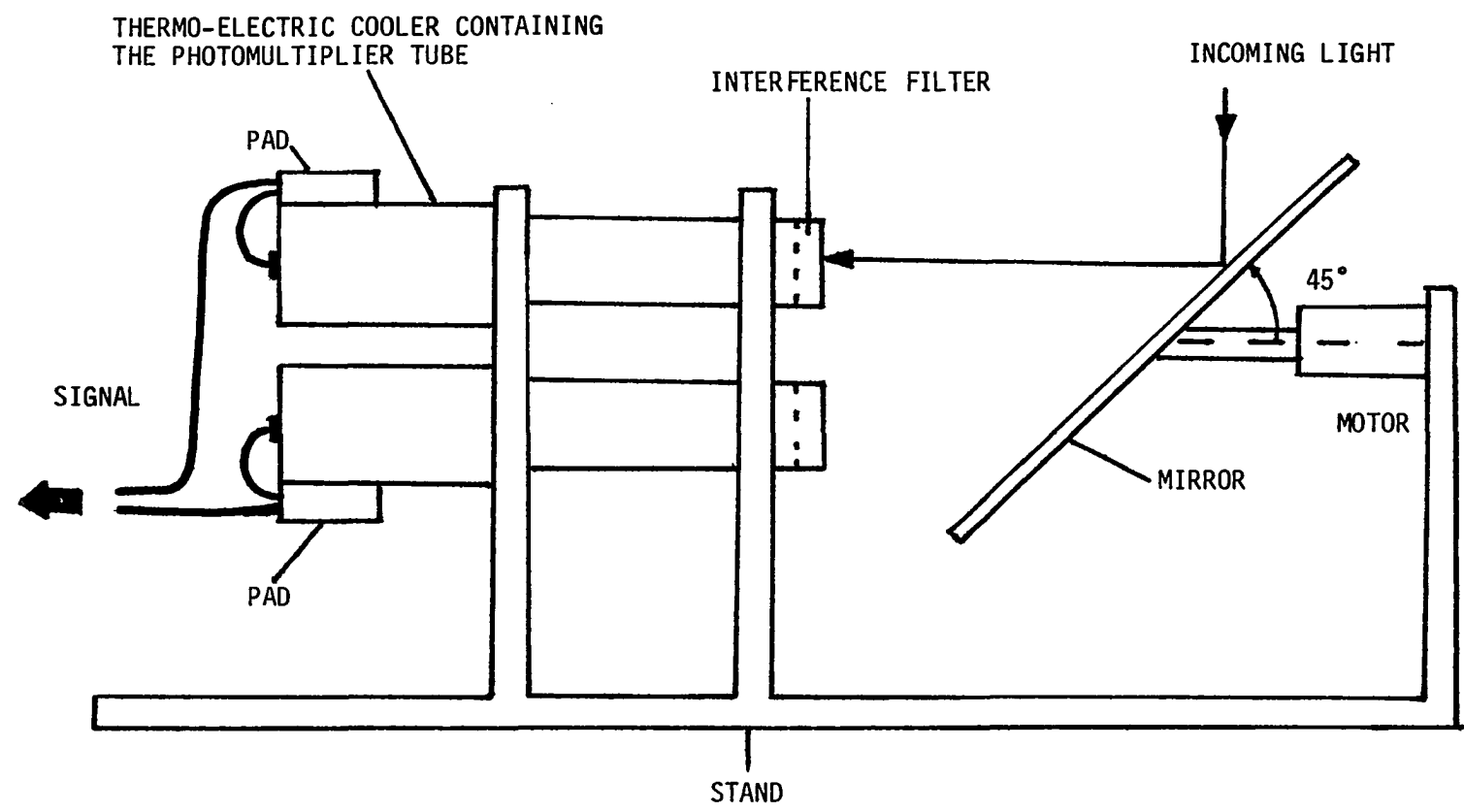


Figure 2.3 The setup of the meridian scanning photometer as viewed from the side.

of N_2^+ at 4278 Å. The light passes into a telescope and is focused on a diaphragm in front of the photomultiplier tube (PMT). As with the spectrometers, the PMTs are housed in thermoelectric coolers which cool the PMTs to -25 degrees centigrade to reduce thermal noise pulses. The signal from the PMT is fed to a pulse-amplifier-discriminator which ignores pulses with voltage levels below a specified threshold. This further aids in eliminating spurious noise pulses due to thermal effects.

Using such a simple instrument design and relatively large-area filters (about 7.5 cm in diameter) provides for a very large throughput. This makes the photometer a useful tool for monitoring weak emissions from relatively small (about 1.5 degree circular) regions of the sky.

2.4 The All Sky Camera

The observing station is equipped with a 35 mm automatic all sky camera (ASC). The camera has a large fish-eye lens allowing a 160 degree view of the sky. Normally the camera takes one 8 second exposure every minute providing visual data throughout the observing period. Several other exposure rates are also available by adjusting the ASC's control box. The camera holds sufficient film to run continuously for a period of 24 hours. The ASC is equipped with a small data box that houses a 24 hour clock (UT) and a small placard showing the UT date, as well as the station identification. The contents of the data box are photographed every exposure and appears in the southeast corner of every frame.

The ASC is housed in the same building as the MSPs where a constant temperature is maintained. A hemispherical glass dome provides a viewing port and protection from the harsh climate for the ASC. When scattered sunlight along the southern horizon is intense or when the full moon is along the horizon a shade is used to block the scattered light. The ASC provides a reliable record of weather conditions and types of auroral forms being observed. It also provides information about the time history of auroral substorms.

2.5 The Data Processing System

Data from the two spectrometers and the four channel MSP are handled by a digital electronic data processing system. The brain of the data collection system is a Nova 800 mini-computer, built by Data General Co. Its 32 K words (16 bit) of magnetic core memory provide temporary data storage and executable program memory during operation. Permanent data storage is provided by a Digi-Data magnetic tape drive which permits twelve hours of data collection on each ten and one half inch diameter tape reel. A block diagram of the data collection system is presented in Figure 2.4. The system permits real-time user interaction through any display terminal with a keyboard, such as the Tektronix 4010 interactive graphics unit. While the computer is accumulating and storing the data scans of the six instruments to which it is connected, the same data may also be copied in three temporary storage buffers of the computer memory and displayed on the terminal. Each data scan for a particular instrument may be displayed individually or several scans may be summed to improve the signal-to-noise ratio.

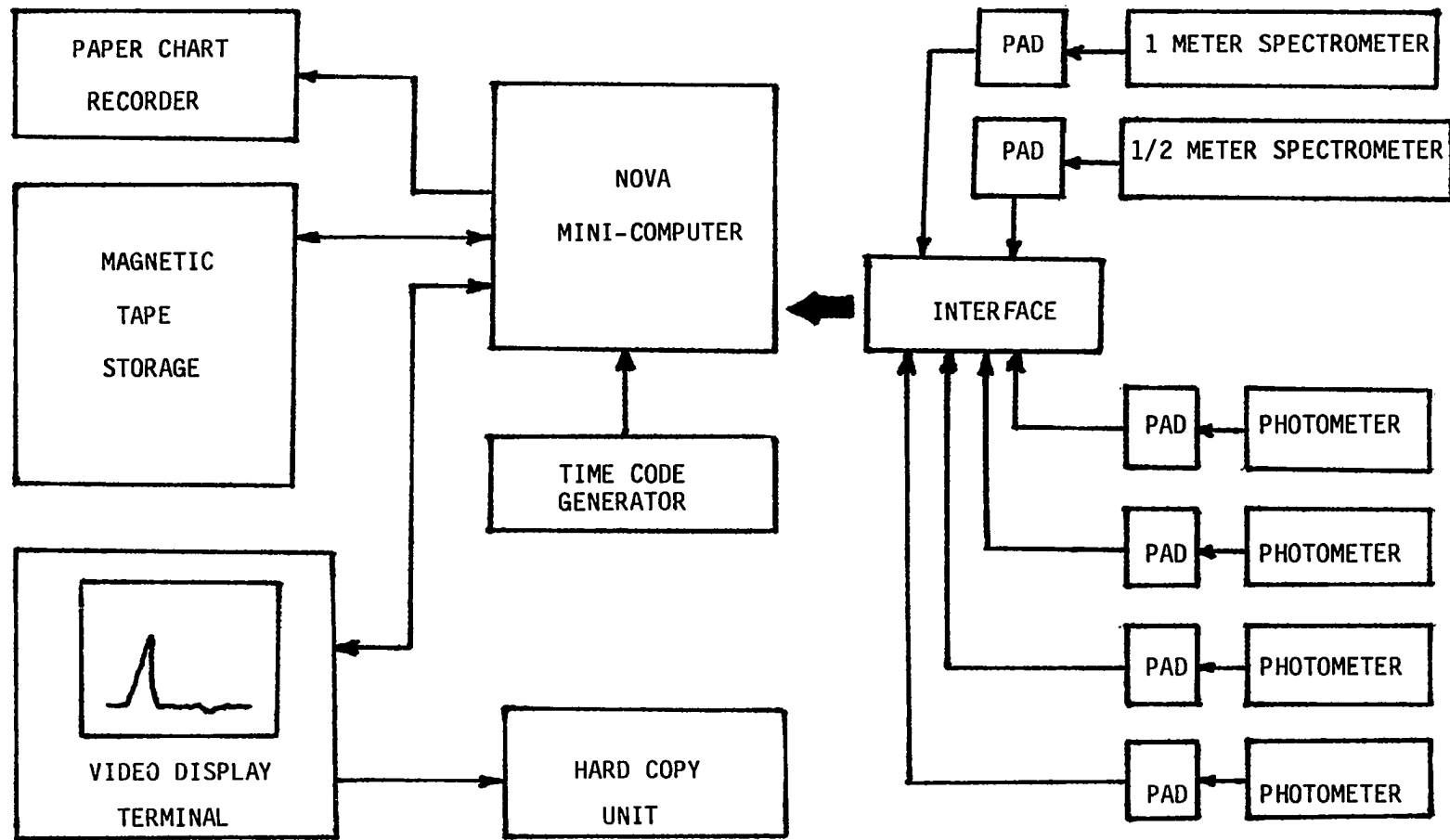


Figure 2.4 A block diagram of the data collection system in Longyearbyen.

The contents of the data buffers may be manipulated through point-by-point addition, subtraction, multiplication, division and cross-correlation by one of the other buffers.

The data are displayed graphically as a plot of photometric signal (in pulse counts) versus wavelength for the two spectrometers. Sample displays of the spectrometer data are shown in Figure 2.5, for the half-meter spectrometer, and Figure 2.6, for the one-meter spectrometer. The display for the meridian scanning photometers is a plot of photometer pulse counts versus elevation angle from the northern horizon. An example of the output from the [OI] 6300 Å photometer is shown in Figure 2.7.

The text on each of the graphs relates information such as what instrument the data originated from, the universal time (UT), the scale of the graph and other specific information about the operation of the detector. The header for the spectrometers includes the wavelength region being scanned and information about the slit width and order sorting filters used. The azimuth and elevation information apply only to the spectrometers even though they are also printed on the MSP display.

The display may be altered significantly to suit the needs of the researcher. Any or all of the wavelength region originally recorded may be displayed. In Figure 2.6 the original scan was from 3435 Å to 3950 Å, however the data can be viewed more easily when displayed from 3435 Å to 3500 Å. The vertical axis of the display may be altered to provide the clearest representation of the intensity and line shapes

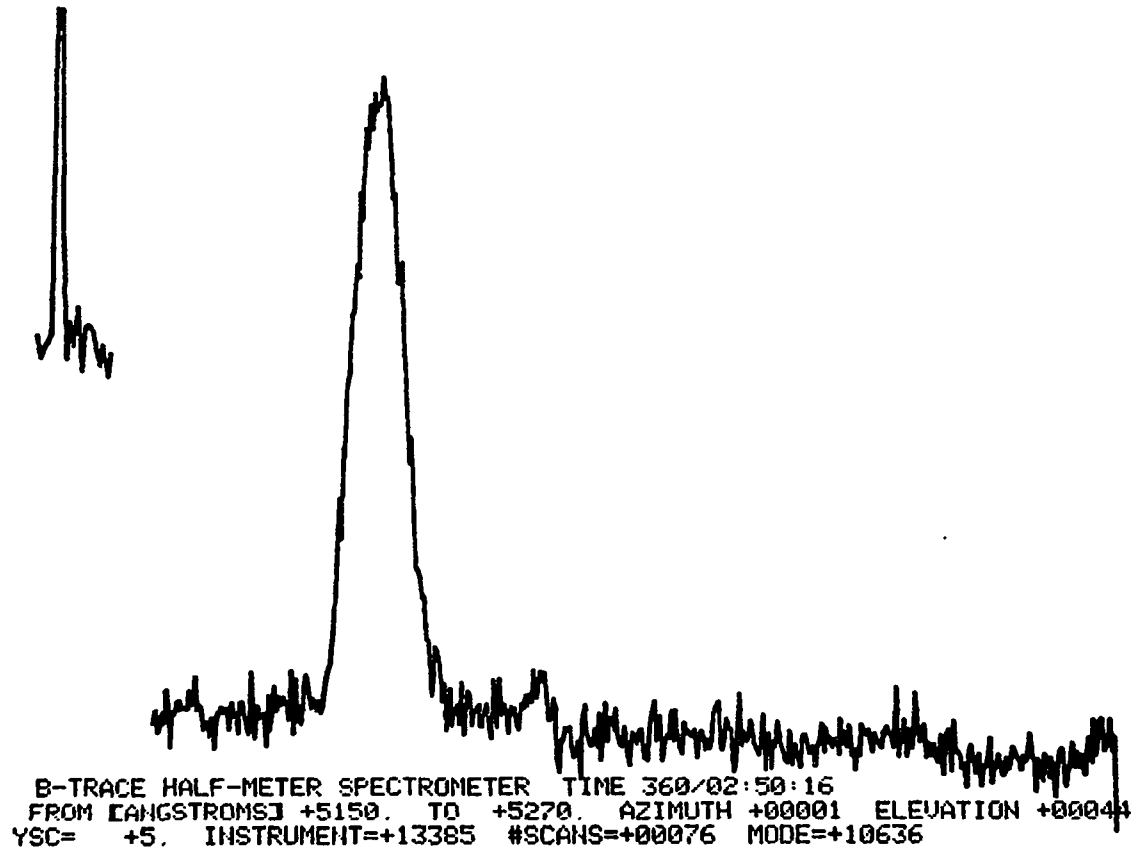


Figure 2.5 Example of the one-half meter spectrometer display (not to scale).

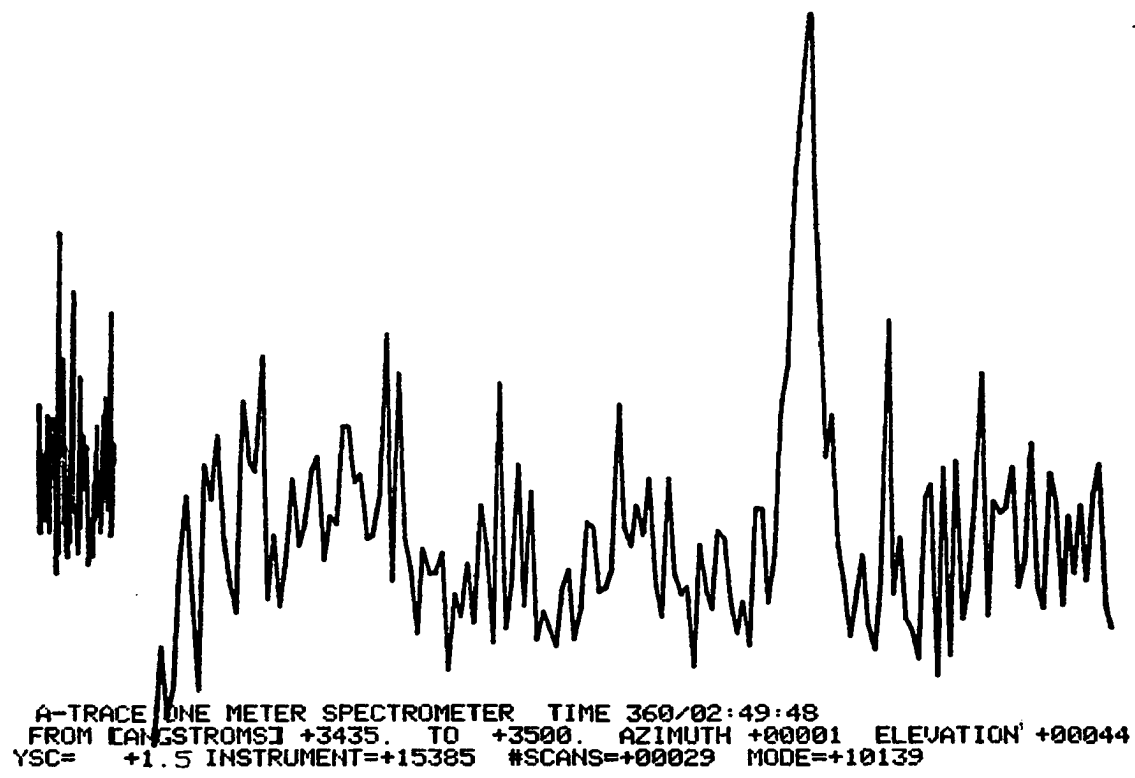


Figure 2.6 Example of the one-meter spectrometer display (not to scale).

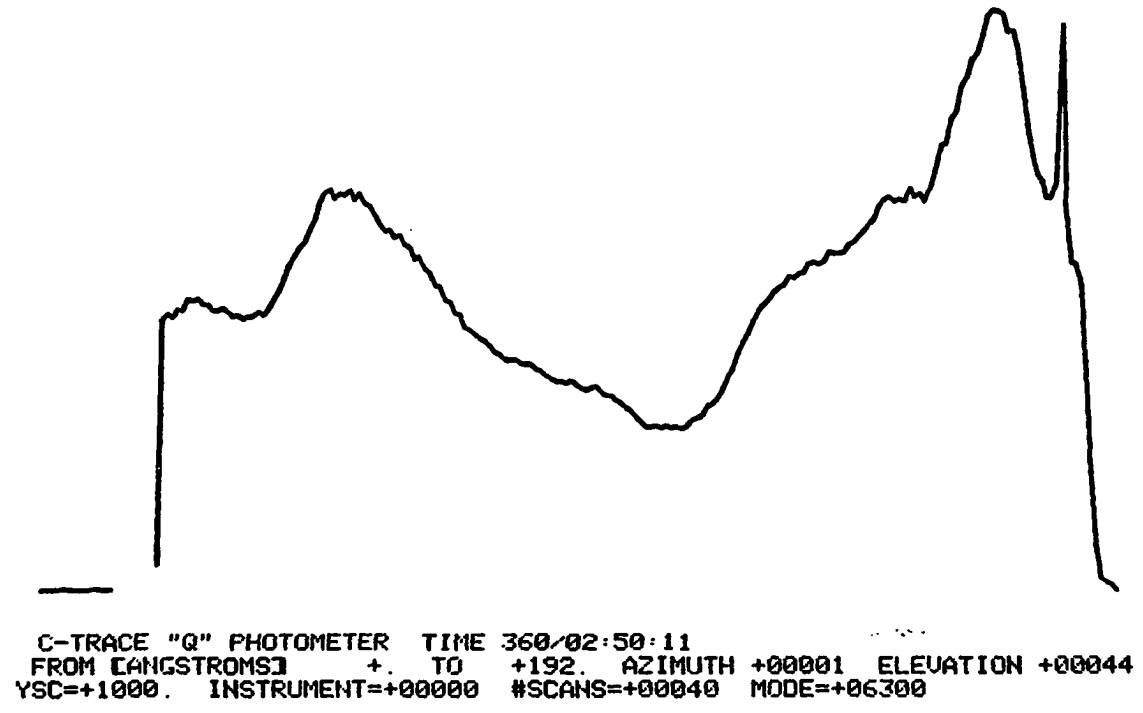


Figure 2.7 Example of the 6300 A meridian scanning photometer display (not to scale).

of interest. Once the desired effect is achieved on the display terminal, the entire screen may be reproduced using a Tektronix 4531 hard copy unit, providing a permanent record of the data.

The computer collects the data from the six separate instruments instantaneously, for all practical purposes. An accurate account of exactly when each scan is taken allows the temporal variations of any of the observed emissions to be studied and correlated with other geophysical and solar data.

CHAPTER 3

OBSERVATIONS AND DATA PREPARATION

3.1 The Objective

The central task in this thesis project was to measure the absolute intensities of optical emissions in $\text{NI}[^2\text{D}]$ and $\text{NI}[^2\text{P}]$ from a large number of auroras excited by particles with average energies varying from less than 0.5 KeV to a few KeV in order to determine the NI populations in these two metastable energy levels. This objective was met by making simultaneous spectroscopic measurements of the $[\text{NI}]$ 3466 Å and $[\text{NI}]$ 5200 Å emissions in auroras occurring over Longyearbyen, Svalbard, around the winter solstice period when it is possible to observe both night-time and mid-day auroral activities. The average energies of the observed auroral particles can be estimated from photometric measurements of $[\text{OI}]$ 6300 Å and N_2^+ 4278 Å emission intensities (Rees and Lucky, 1974). Both spectroscopic and photometric measurements of auroral emissions made in Longyearbyen are presented in this chapter. The procedure for the absolute calibration of these detectors is also described. The final section of this chapter is devoted to the analysis of the spectroscopic and photometric data taken in Longyearbyen.

3.2 The Observing Program

The main observing season in Longyearbyen runs from late November into late January when the solar depression angle is always greater than nine degrees. During the 1979-1980 observing season the

3466 Å, 5200 Å observations were made for approximately two weeks, from December 24, 1979 to January 7, 1980. The full moon occurred on January 2, 1980, so much of this period had a large percentage of moon-up time. This did cause scattered light problems with the MSP but did not appreciably effect the spectrometer data, except under aurorally quiet conditions when the [NI] 3466 Å and [NI] 5200 Å emissions were extremely weak (less than 5 rayleighs). The MSP was run continuously except when the sky was totally obscured by clouds or when intense background light overpowered the observable emissions. The relative stability and position of any auroral activity could be easily monitored by observing the MSP record which produced three scans per minute of the magnetic meridian. The spectrometers were usually directed toward the brightest, most stable auroral feature in the sky. These were often bright arcs around the zenith which were relatively stable for periods of a half hour or more. During mid-day when the auroral activity was low, a slowly moving photometric 6300 Å feature believed to be the optical signature of the magnetospheric cusp, provided very low energy electron data for the spectrometers. This feature was sub-visual and could only be located using the MSP record. Rapidly changing auroras such as those associated with an auroral break-up were not of any interest in this study since they did not meet the conditions of stability necessary for a realistic ratio of the two emissions for [NI] 3466 Å and [NI] 5200 Å with such different effective lifetimes.

Adverse weather conditions are common in Longyearbyen during the

winter, often limiting the amount of data which may be collected. During the observing period, cloud cover and blowing snow limited data collection to just seven days; December 25, 26, 27 and 29, 1979 and January 2, 5 and 6, 1980. Periods of slight haze and patchy clouds affected a significant part of these data, the effects of which are discussed in section 3.6.

The 3466 Å doublet was recorded on the one-meter spectrometer by scanning the third order from 3435 Å to 3950 Å using a 1 mm slitwidth which corresponds to an emission line halfwidth of about 2 Å. The one-meter spectrometer used a 32 second scan period. A pulse-integration period of 25 milliseconds was adopted to preserve the inherent resolution of the data. Each scan consists of 1280 spectral elements. Scanning a 515 Å wide wavelength region at about 2 Å resolution produces about 257 resolution elements. The 1280 spectral samples thus preserve the resolution of the data since they provide five spectral samples per resolution element.

The 5200 Å doublet was recorded on the half-meter spectrometer by scanning the second order from 5150 Å to 5270 Å with a 1 mm slitwidth. The 6 Å resolution of the half-meter spectrometer does not resolve the two peaks of the 5200 Å doublet. However this is not considered a problem since the ratio of the two can be determined (see section 3.6). A scan period of 12 seconds is employed on the half-meter spectrometer with a 25 millisecond integration period thereby producing 480 spectral elements per scan. Since a 120 Å wavelength region is covered during each scan, the 6 Å resolution provides for 20 resolution elements.

The inherent resolution of the data is easily preserved with about 24 spectral elements composing each of the resolution elements.

3.3 Field Calibration Procedures

Two types of calibration are routinely performed during the observing season: absolute intensity calibration of the spectrometers and the photometers, and wavelength calibrations of the spectrometers.

The absolute intensity calibration employs a quartz iodide lamp with known spectral intensity characteristics. The lamp is placed a measured distance from the instrument being calibrated and a lambertian surface, large enough to fill completely the instrument's FOV, is used to scatter the light into the instrument. Several scans are monitored and recorded on a magnetic tape. A logbook entry including the procedure, distance from the lamp to the screen, the angle of the screen to the optical axis of the instrument and the exact universal time (UT) the scans were taken, is made. The calibration for the spectrometers is complicated due to the different combinations of order-sorting filters and slitwidths that may be used to observe different wavelengths. In order to ensure an accurate calibration, each combination of filters and slitwidth used for taking data must be calibrated separately. The logbook entry and information coded on the magnetic tape record of each scan must relate the exact time that a scan with a particular combination was taken. The largest cam, yielding the greatest change in grating angle, is generally used during calibrations to simplify the procedure by allowing a larger wavelength region to be scanned at one time.

Using spectral lamps, a wavelength calibration is performed on the spectrometers in order to identify the important features and scale the wavelength axis of the data display. The wavelength calibration also provides a check on the optical alignment of the spectrometers as indicated by the instrumental halfwidths of the monitored emission lines. For this calibration, a lamp containing one or more elements that emit bright, sharp and well documented emission lines is used. The lamp must have at least two well-spaced features in the wavelength region being calibrated (or in another detectable order of the wavelength region) in order to scale the wavelength axis. For this reason, the particular lamp used depends on the wavelength region under study. A neon lamp was used to calibrate both the one-meter spectrometer around 3466 Å and the 5200 Å region on the half-meter spectrometer. Neon has several strong emission lines around 3466 Å which are detected in the third order by the one-meter spectrometer. These same lines may be detected around 5200 Å in the second order on the half-meter spectrometer and used for the 5200 Å calibration. This does require the removal of the order sorting filters on the half-meter spectrometer, but it does not affect the wavelength calibration. As with the intensity calibrations a log entry is made to document the wavelengths calibrated, type of lamp used and the UT time the scans were taken.

3.4 Absolute Intensity Calibration

The absolute intensity of an emission is determined by comparing its signal to that of a source of known spectral brightness. To accomplish this, a factory-calibrated lamp is used. The quartz iodide

lamp used in these calibrations had its irradiance versus wavelength characteristics measured at the factory when it was produced in 1970. This differential irradiance was measured in micro-watts/cm²/10Å (erg/cm²/Å/sec) at a distance of 40 cm and operating at a lamp current of 6.5 amperes. This information was provided by the manufacturers in the form of a graph of irradiance versus wavelength, over a wavelength region from 2600 Å to 26000 Å. The irradiance must be converted to units of surface brightness (rayleighs, R) since, for calibration purposes, we need surface brightness rather than irradiance. We can make use of the basic relationship between energy and wavelength to relate total energy, E, of light at a wavelength λ to the number of photons, N, of this light:

$$N = E\lambda/hc \text{ photons/cm}^2/\text{sec}/\text{Å} \quad (3-1)$$

where h is Planck's constant and c is the velocity of light in a vacuum. If we allow these N photons to be uniformly scattered from a lambertian surface into a hemisphere, then the number of photons scattered by the surface in any direction is:

$$N' = E\lambda\cos\delta/hc\pi \text{ photons/cm}^2/\text{sec}/\text{sterad}/\text{Å} \quad (3-2)$$

Where δ is the angle between the incident light and the screen normal. The rayleigh is 10⁶/4π photons/cm²/sec/sterad so the screen brightness is:

$$SB = 4\pi N'\cos\delta/10^6 = 4E\lambda\cos\delta/10^6hc \text{ R}/\text{Å} \quad (3-3)$$

Since the intensity varies as the inverse of the distance squared and E is given in micro-watts/cm²/10Å with λ given in Angstroms, the brightness of the screen placed at a distance d (in cm) from the lamp

becomes:

$$SB = 201.2 E\lambda(40/d)^2 \cos\delta \quad R/\text{\AA} \quad (3-4)$$

Where d is the distance from the light source to the screen, in cm.

This screen brightness must be multiplied by the instrumental halfwidth (HW) at the desired wavelength in order to express the intensity in rayleighs. A determination of the instrumental halfwidth at the 3466 Å, 3914 Å and 5200 Å wavelengths was made using the wavelength calibration from day 361, 1979. The halfwidths were measured directly from the neon emission lines on the pulse count versus wavelength display. A value of 5.85 ± 0.15 Å was determined for the halfwidth of the 5200 Å emission on the half-meter spectrometer. This agreed very well with the calculated resolution at this wavelength (5.88 Å) for a half meter focal length spectrometer employing a 1200 groove per mm grating and a 1 mm slitwidth. The halfwidth of the 3466 Å emission was measured to be 2.20 ± 0.15 Å on the one-meter spectrometer. This is slightly larger than the theoretical dispersion of 1.95 Å/mm. The bandpass for the photometers is the measured halfwidth of the interference filter's transmission. The 6300 Å photometer had a halfwidth of 15.4 Å and the 4278 Å photometer had a 15.9 Å bandpass.

The field calibration signal is recorded in units of pulse counts for a known screen brightness, determined in rayleighs. A calibration factor is obtained by dividing the intensity in rayleighs by the number of pulse counts measured. This value is typically different for every emission being observed.

The error associated with the calibration factor is the result of inaccuracies in several measured quantities (details in Appendix):

- 1) The error in the quartz iodide lamp's irradiance versus wavelength calibration has been checked against an N.B.S. calibrated light source and varies by no more than $\pm 5\%$ (Romick, G., private communication).
- 2) The error in the distance measurement between the lamp and the lambertian screen of ± 0.1 m results in less than $\pm 2\%$ error for d^2 in all cases.
- 3) The inaccuracy in the measurements of the angle, δ , between the screen normal and the direction of the incident light is less than ± 5 degrees. Allowing for this variation in screen angle the associated value for $\cos\delta$ is accurate within $\pm 17\%$ for the one-meter spectrometer, $\pm 4\%$ for the one-half meter spectrometer and within $\pm 9\%$ for the MSP.
- 4) The signal pulses from the PMT occur randomly so the statistics for the instrumental error, AC (in percent), is:

$$AC = \pm 100 \times (P)^{1/2} / P$$
 Where P is the number of pulse counts in the calibration. For the 3466 Å emission the pulse count is accurate within $\pm 12\%$, within $\pm 9\%$ for 3914 Å and it is within $\pm 1.5\%$ for the 5200 Å and 6300 Å emissions.
- 5) The error of the measured instrumental halfwidths is less than $\pm 9\%$ for the one-meter spectrometer, less than $\pm 4\%$ for the half-meter spectrometer and within $\pm 2\%$ for the

6300 Å photometer.

- 6) The error involved in the correction for atmospheric extinction (see section 3.5) is within $\pm 15\%$ for the value of the correction factor.

Using standard error propagation techniques for independent errors (Beers, 1953), the total accuracy of the calibration values were determined to be $\pm 26\%$ for the one-meter spectrometer, $\pm 17\%$ for the half-meter spectrometer and for the 6300 Å photometer the error is within $\pm 18\%$.

The calibration for the 3466 Å and 3914 Å emissions was made on day 329, 1979, at a distance of 18.4 m, with $\delta = 62.5$ degrees. These data resulted in calibration factors of 2.4 ± 0.6 R/count for 3466 Å and 1.9 ± 0.5 R/count for the 3914 Å emission, including a correction for atmospheric attenuation (section 3.5). During the field calibrations of the 1979-1980 season, the 5200 Å region with the particular filter combination used in the observations was not calibrated. Fortunately measurements of this same wavelength region with the same filter combination, at the same slitwidth were made during the 1978-1979 observing season. It is reasonable to assume that the instrument did not degrade appreciably in one year of service and this is borne out by comparing spectra from both seasons. Therefore the calibration was taken from day 003, 1979, at a distance of 20.75 m, with a screen angle of 25 degrees. The calibration factor for the 5200 Å emission was determined to be 1.5 ± 0.3 R/count.

Scattered background light, such as scattered moonlight, made

intensity measurements for the photometer data troublesome by increasing the difficulty of determining a proper baseline for the emissions. The 4278 Å photometer data was particularly error-prone, being much weaker than the 6300 Å emission. For this reason the 3914 Å emission was used to determine the amount of 4278 Å emission present. These two emissions may be related to each other by their Frank-Condon factors, both being emitted by the same electronic and vibrational excited state of N_2^+ ; the ratio of the Frank-Condon factors for 3914 Å and 4278 Å is 0.305. Including this result, the calibration factor for 4278 Å, in terms of 3914 Å counts, is 0.59 ± 0.15 R/count.

The photometer calibration for 6300 Å was taken on day 329, 1979, at a distance of 26.4 m with a screen angle, δ , of 45 degrees. The calibration is accomplished in the same way as for the spectrometer data except that a correction is required due to the large intensity of the calibration 6300 Å emission. The pulse-amplifier-discriminator (PAD) experiences a pulse-pileup when the count rate exceeds 200,000 counts/sec and as a result, the device becomes nonlinear. The PAD has been calibrated in the laboratory by monitoring both the analog output of the PMT using a picoammeter and digital pulses going into the PAD to account for this behavior at high count rates. This calibration curve was used to correct the high count rate from the 6300 Å photometer during the absolute intensity calibration procedure. The operation of the PAD under normal conditions is linear so this correction is only necessary for this calibration. A calibration factor of 0.23 ± 0.04 R/count was found for the 6300 Å photometer.

3.5 Atmospheric Extinction

As any emission travels from its origin to the detector, some of it is absorbed leaving only a fraction of the initial intensity (I_0) to reach the instrument. The intensity of an emission passing through an absorbing gas layer can be expressed as:

$$I = I_0 \exp[-kh \sec \beta] \quad (3-5)$$

So the original emission can be expressed;

$$I_0 = I \exp[kh \sec \beta] \quad (3-6)$$

where k is the extinction constant due to absorption and scattering, h is the thickness of the absorbing layer, β is the zenith angle and I is the intensity as seen by the instrument. Values for kh , based on the 1962 U.S. Standard Clear Atmosphere, can be found in the Handbook of Geophysics and Space Environments (1965) as total optical thickness parameters.

The 3466 Å and 5200 Å emissions received by the instruments originate at altitudes exceeding 100 km. Nearly all of the absorption of these emissions occur in the troposphere so, to a very good approximation, all of the emissions can be assumed to pass through the entire absorbing layer. In this way, a correction factor can be determined to remove the effects of absorption. In this study it has been assumed that the dependence of the absorption of an emission on β is negligible due to the increase in signal from resonant scattering. This assumption can be checked by comparing the 5200 Å to 3466 Å ratios observed at the different values of β . With this assumption, the correction

factor is:

$$CF = \exp[kh] \quad (3-7)$$

The actual values for kh were determined by linearly interpolating the published tabular values mentioned above. This results in a correction factor of 1.950 for the 3466 Å emission, 1.135 for the 5200 Å emission, 1.480 for the 3914 Å emission and 1.059 for the 6300 Å emission. These factors have been incorporated into the absolute intensity calibration values presented in section 3.4.

3.6 Data Analysis

The auroral optical measurements made in Longyearbyen are stored on magnetic tapes. The spectroscopic data of the relatively weak [NI] 3466 Å and 5200 Å emissions were played back from the magnetic tape into the computer for analysis. In an effort to improve the signal-to-noise ratio of the data, individual scans were summed for 15 minute intervals. For the most part, the auroral forms observed were relatively stable over this time period with some exceptions noted below. A typical sum over a 15 minute interval covered 28 scans of the one-meter spectrometer and 65 scans of the half-meter spectrometer.

Not all of the collected data accurately describes the variations of the 3466 Å and 5200 Å emissions. The 3466 Å ultra-violet (UV) doublet is very strongly absorbed by any haze or clouds while the 5200 Å emission is only mildly affected. For this reason data taken when any haze or clouds were present must be rejected to avoid an artificially high 5200 Å to 3466 Å emission ratio. Such points

were identified in the all-sky camera data and logbook entries during the observing periods. A second source of error in determining the 5200 Å to 3466 Å ratio is the radiative lifetime of the 5200 Å emission which is much longer than that of the 3466 Å emission. The measurements rely on the assumption of a steady state which is not attained during a rapidly (faster than the effective lifetime of $\text{NI}[^2\text{D}, ^2\text{P}]$) changing particle flux. As a result, the intensity build-up of the 5200 Å emission is slower than the 3466 Å emission, yielding an artificially low 5200 Å to 3466 Å intensity ratio. By checking the 15 minute sum of scans for a few individual scans that are much more intense than the rest, these points may be singled out and eliminated. Cloud coverage during observation periods was determined by visual search of the all sky camera films. However it was often questionable whether any thin, subvisual haze was present or not, or if a moderately rapid excitation occurred. If a clear distinction could not be made, the questionable points were not removed in an effort to keep the data as unbiased as possible.

The raw data taken from magnetic tape is displayed graphically as pulse counts versus wavelength for the spectrometers and pulse counts versus elevation for the photometers. The intensity of each emission feature on the graph is scaled in counts per inch of chart. The scaling factor, YSC in Fig. 2.5, 2.6 and 2.7, multiplied by the height of the emission feature on the chart yields the number of counts associated with that emission. Alternatively, the total number of counts associated with a particular emission feature may be obtained

from a computer readout. In order to measure the intensity of an emission above the background, a baseline must be drawn to subtract any background light present. For strong emissions with large signal-to-noise ratios this is not necessary. During quiet periods, however the signal-to-noise ratio can approach unity on the spectrometer output so the choice of baselines may effect the intensity measurement by as much as 20%. Particular care must be exercised if the emission occurs on top of a background auroral emission which may, or may not be present, depending on auroral conditions. The effect is pronounced in the 3466 Å data during quiet periods where scattered light is present. Determining a baseline for the photometer data is not difficult for bright arcs located near the zenith but broad bands near the horizon may cause problems. If scattered sunlight is strong, an effective baseline is difficult to determine as it can blend in with any broad emissions near the horizon. The error in the photometer data is believed to be less than 50% even under poor conditions.

The intensities of the spectrometer and photometers are correlated by taking the photometer's intensity value at the same elevation at which the spectrometers are set. This is not valid at all times since the spectrometer does not always view the magnetic meridian. Each graph of a 15 minute sum produces one intensity measurement, a data point. Approximately 200 such data points were taken for each of the 3466 Å, 5200 Å, 4278 Å and 6300 Å emissions.

The raw data were plotted as the intensities of 5200 Å versus 3466 Å emissions and a least squares linear regression was used to

compute a best fit straight line. A plot of the 5200 Å versus 3466 Å intensities utilizing all the available data points is shown in Figure 3.1. The intensities are expressed in rayleighs. The best fit line has a slope (the 5200 Å to 3466 Å ratio) of 1.62, the y-intercept is 4.3 and the correlation coefficient is 0.920 (± 1 is a perfect fit). The non-zero y-intercept seems to indicate that a significant amount of 5200 Å radiation is present when no 3466 Å light is produced. After removing data points identified as measurements taken under cloudy or non-equilibrium conditions, the reduced data was replotted (see Figure 3.2). The scatter is reduced considerably but the slope of the best fit line does not change radically, now having a value of 1.84. The y-intercept does change significantly to a value of -0.2 and the correlation coefficient has improved to a value of 0.975. A calculation of the root-mean-square (RMS) deviation of the reduced data was undertaken to estimate the accuracy of the 5200 Å to 3466 Å intensity ratio determined above. An RMS deviation of ± 0.40 was calculated, making the ratio 1.84 ± 0.40 . The zero point 5200 Å off-set is no longer apparent in the data (within the error), indicating that the two excited states are produced by the same primary source in the aurora.

The intensities of the 6300 Å and 4278 Å emissions were taken in an effort to provide some information about the characteristic particle energies during the observations. The spectral energy distribution of primary auroral electrons is frequently observed to have a Maxwellian functional form (Rees and Luckey, 1974):

$$N(E)dE = N_0 E \exp(-E/\alpha) dE \quad \text{electron cm}^{-2} \text{ sec}^{-1} \text{ eV}^{-1}$$

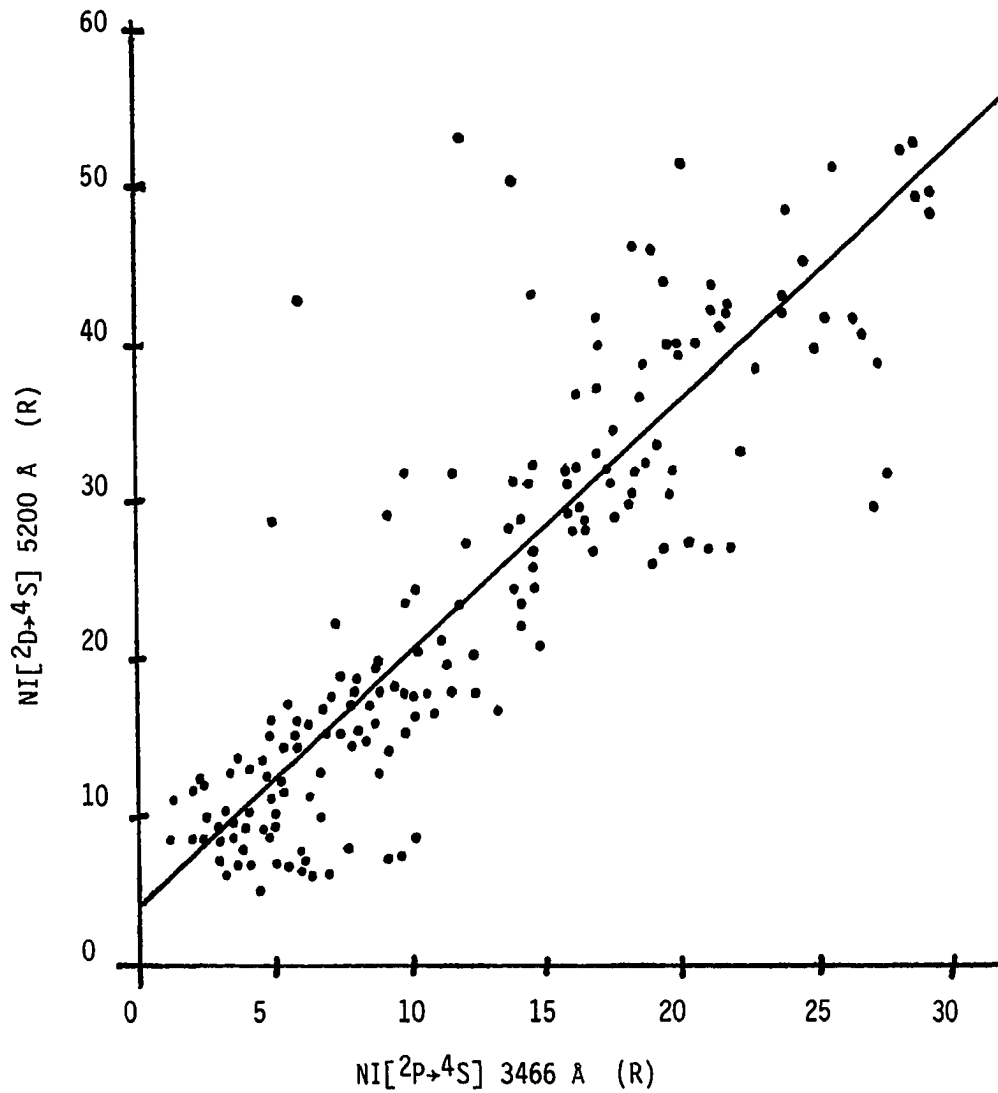


Figure 3.1 A plot of the raw 5200 Å versus 3466 Å data. The slope of the best fitting line is 1.62 and the line intersects the 5200 Å axis at 4.3 R.

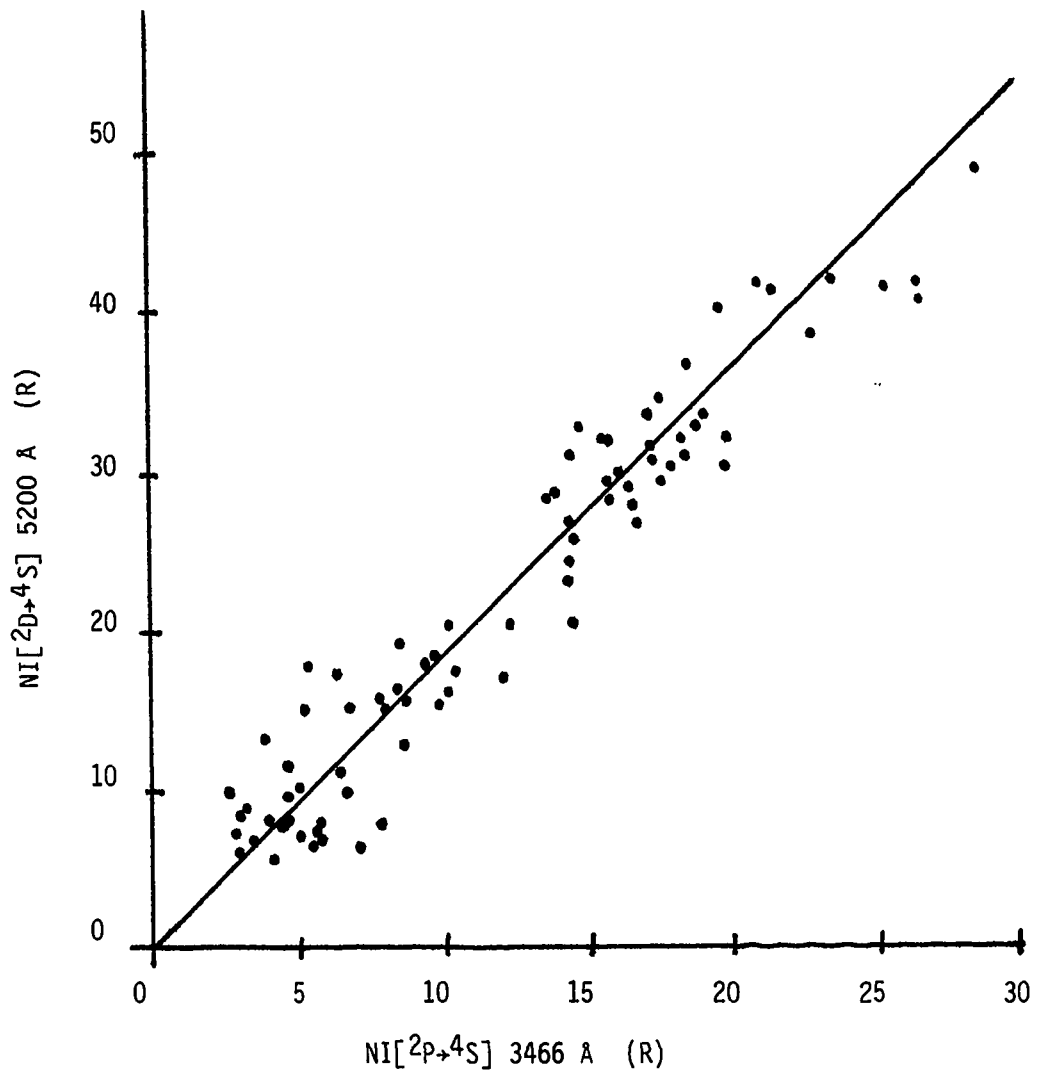


Figure 3.2 A plot of the reduced 5200 Å versus 3466 Å data. The slope of the best fitting line is 1.84 and the line intersects the 5200 Å axis at -0.2 R.

where N_0 is the total number of electrons, E is the energy of the electron and α is the characteristic energy of the Maxwellian, occurring at the peak of the distribution curve. Observing 6300 Å and 4278 Å emissions, Rees and Lucky (1974) related their ratio to the characteristic energy α .

The data were plotted as 6300 Å versus 4278 Å intensities (see Figure 3.3) in order to use the results of Rees and Lucky to estimate the range of characteristic energies of the primary particles producing the observed emissions. Most of the night-time data were from aurorally very quiet periods so no reliable values resulted. Several trends were apparent in the analysis of the day-time data points however. The inferred characteristic energies of the precipitating electrons ranged from less than 0.5 keV up to about 2.5 keV. Typical night-time auroras have characteristic energies of about 5 keV. When the upper atmosphere is sun-lit, part of the 4278 Å contribution is due to resonant scattering so α is actually over-estimated. This is because Rees and Lucky's results are only valid for electron impact sources of 4278 Å and 6300 Å emissions. The higher characteristic energies appeared to be associated with bright, distinct arcs while the lower energies tended to be associated with the very broad auroral features. Comparison of the 5200 Å to 3466 Å ratio with the 6300 Å to 4278 Å ratio on a point-by-point basis indicates a weak positive dependence of the [NI] ratio on the characteristic particle energy, but the variation was within the error bars so no valid conclusion could be made.

As previously mentioned, the 5198.5 Å and 5200.7 Å emissions that

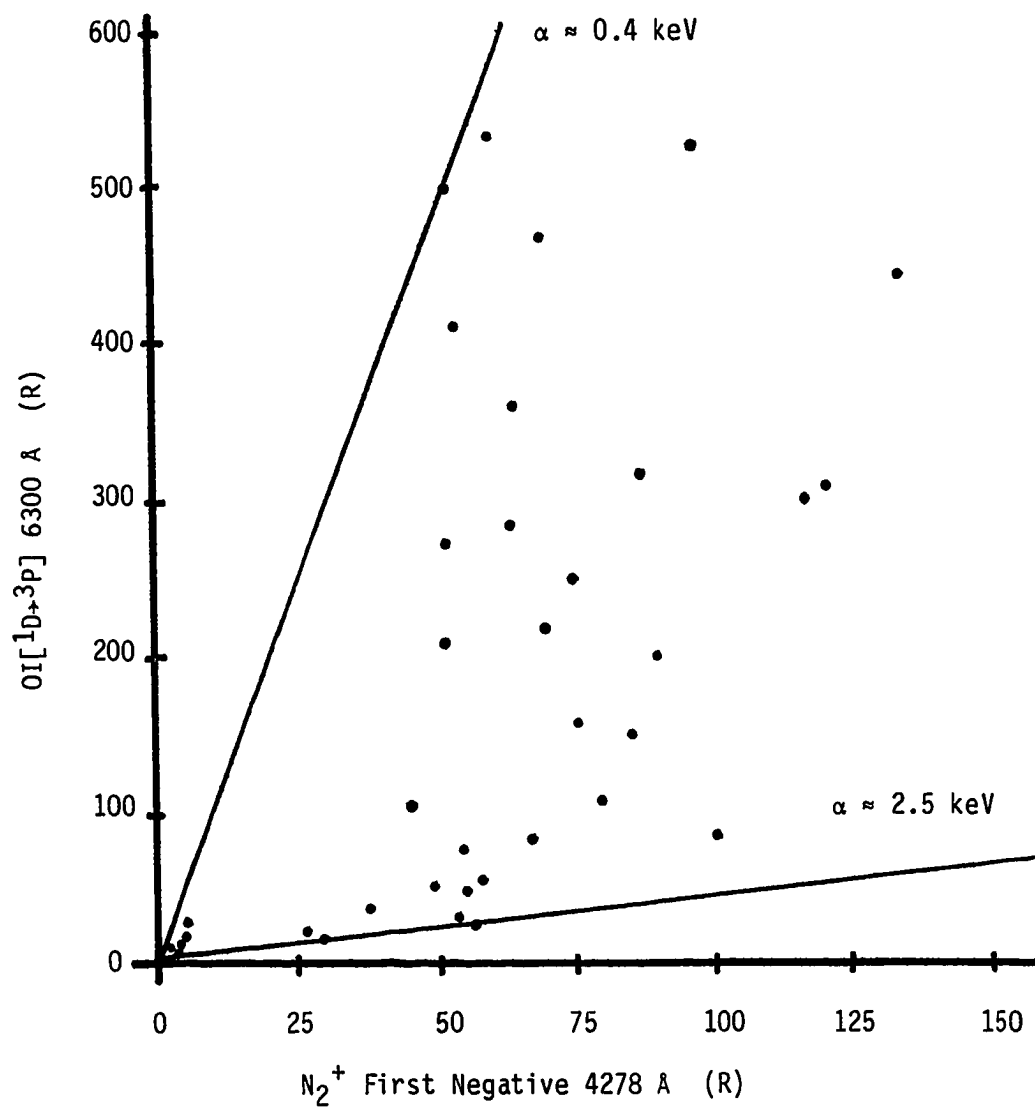


Figure 3.3 A plot of 6300 Å versus 4278 Å data points, made in order to estimate the range of characteristic energies in the auroras observed.

make up the 5200 Å emission has been found to vary in some high altitude auroras (Sivjee et al, 1981). The 5198.5 Å to 5200.7 Å ratio ranges from 1.56, for night-side auroras, to 1.20 during some day-side auroras. For comparison purposes, it is useful to identify what the predominant ratio is in the observed data. By adding two triangle functions spaced 2.2 Å apart, with the same halfwidth as the half-meter spectrometer (5.85 Å), and comparing the resulting halfwidth with several measured halfwidths of the data, most of the data appear to have 5198.5 Å to 5200.7 Å ratios of 1.6 ± 0.2 . This would be consistent with the normal night-side variety and should be directly comparable to most other auroral studies.

CHAPTER 4
ATOMIC NITROGEN IN THE AURORA

4.1 Modeling the Excited States of Atomic Nitrogen

The main objective of the measurements presented in Chapter 3 is to provide a comparison for model calculations which derive population rates of NI[²D] and NI[²P] in the aurora. The need for these model calculations arises from the nature of the electronic transitions which lead to the 3466 Å and 5200 Å emissions.

All optical emissions are due to an excited species undergoing either permitted or forbidden transitions to lower energy states. Permitted transitions occur in very short periods of time (about 10⁻⁸ seconds) so the effects of collisional deactivation in the tenuous upper atmosphere may be neglected. In these transitions the intensity (I) of the emission is directly proportional to the population of the excited state:

$$I_{ij} = [X(i)]A(i,j) \quad (4-1)$$

Where [X(i)] is the concentration of species X and A(i,j) is the Einstein transition probability from state i to state j.

On the other hand, if the transition probability (sec⁻¹) of an excited energy state is comparable to, or less than, the local collision frequency, the above relation must be modified to include quenching effects. These depend on both the quenching rate and the population of the quenching agent and neither of these quantities are well known. In addition, the production rates of the excited states

for various means of production must be taken into account. Modeling, therefore, involves the comparison of a number of probable situations in an attempt to fit the experimental data. While intricate theoretical modeling is beyond the scope of this thesis project, an attempt will be made to review the essential elements of such a model. The results of measurements in Chapter 3 will be compared and contrasted with theoretical calculations reported in the literature in an attempt to determine what improvements are necessary to reconcile the theory with the measurements.

4.2 Atomic Nitrogen in the Auroral Atmosphere

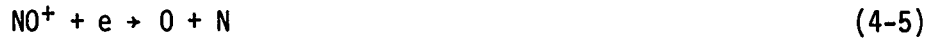
Precipitating electrons in the aurora interact with molecular nitrogen, N_2 , through three major processes which lead to the production of atomic nitrogen.

Auroral electrons produce atomic nitrogen by ionizing N_2 (equation 4-2), followed by a dissociative recombination reaction (equation 4-3), (Hyman et al, 1976):



Reaction 4-3, is exothermic and releases 5.8 eV in excess energy. This excess energy is sufficient to produce NI both in the [2P] and [2D] states. Presently however, the relative amounts of NI atoms produced in the 4S , [2D] and [2P] states through this process have not been determined (Rees, 1975). N_2^+ reacts with O also, producing N and NO^+ . NO^+ then dissociatively recombines to form O and N:





These two reactions do not provide enough excess energy to form $\text{NI}[^2\text{P}]$ but do form $\text{NI}(^4\text{S})$ and $\text{NI}[^2\text{D}]$. The relative abundances of $\text{NI}(^2\text{S})$ and $\text{NI}[^2\text{D}]$ due to these reactions are still unknown (Hyman et al, 1976; Torr et al, 1976).

The second process for atomic nitrogen formation in auroras is through dissociative ionization of N_2 :



Atomic nitrogen can be formed in any of the ^4S , $[^2\text{D}]$ or $[^2\text{P}]$ states in this reaction. Recent rocket observations of $[\text{NI}]$ 3466 Å auroral emission, combined with other laboratory measurements and model calculations yielded values of 0.135, 0.165, 0.300 and 0.400, respectively, for the relative abundances of N^+ , $\text{NI}[^2\text{P}]$, $\text{NI}[^2\text{D}]$, and $\text{NI}(^4\text{S})$ (Zipf et al, 1980). The N^+ ion formed in reaction 4-6 then reacts with O_2 to form NO^+ :



The NO^+ dissociatively recombines with e to form $\text{NI}(^4\text{S})$ and $\text{NI}[^2\text{D}]$ through reaction 4-5.

The third process utilizes the precipitating electron energy to form atomic nitrogen through the dissociation of N_2 :



This reaction also produces $\text{NI}(^4\text{S})$, $\text{NI}[^2\text{D}]$ and $\text{NI}[^2\text{P}]$ and was included in the study by Zipf et al (1980).

Almost half of the precipitating electron energy in auroras is expended in the above reactions and ultimately produces odd nitrogen

species. Nearly all of the remaining auroral electron energy is used up ionizing O_2 and O . There are some reactions involving N_2 and the ions of molecular and atomic oxygen that do produce atomic nitrogen:



The NO^+ dissociatively recombines through reaction 4-5 to produce $NI(^4S)$ and $NI[^2D]$. O_2^+ can also interact with N_2 to form NO^+ and NO :



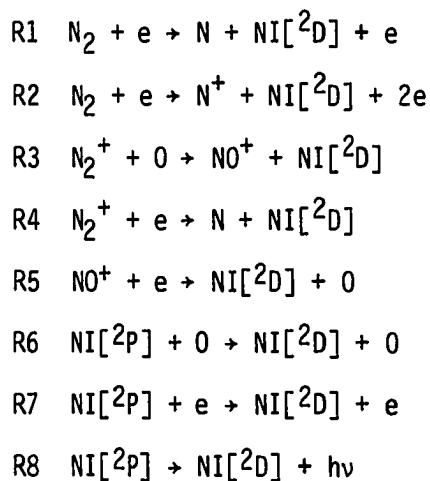
The NO^+ then produces $NI(^4S)$ and $NI[^2D]$ through reaction 4-5. Several of the major reactions which produce and depopulate $NI[^2D]$ and $NI[^2P]$ are presented in Table 4.1 and Table 4.2, respectively.

Not all of the $NI[^2D]$ and $NI[^2P]$ produced actually radiates excess electronic energy. Most of this energy is lost when the $NI[^2D]$ and $NI[^2P]$ combine with O_2 and NO , forming new species, or interacting with O converting the excess energy into the translational energy of both O and N . The major quenching reactions for $NI[^2D]$ are listed in Table 4.1 and for $NI[^2P]$ in Table 4.2. The two major quenchers for both species are O_2 and O . The most important quencher of $NI[^2D]$ depends on the altitude in the atmosphere. O_2 is the dominant quenching agent for altitudes up to about 200 km but O becomes increasingly important with altitude, the concentration of O exceeding that of O_2 above 120 km. A significant portion of the 5200 Å emission is produced above 120 km where atomic oxygen is an increasingly important quenching agent. The quenching effect of O on $NI[^2D]$ is about equal to the effect produced by O_2 at about 200 km. The major quenching agent for $NI[^2P]$ has been found to be atomic oxygen (Torr et al, 1976;

TABLE 4-1

Production and loss mechanisms for the NI[²D] state, which emits the 5200 Å doublet.

Production Mechanisms



De-excitation Mechanisms

Rate Constants

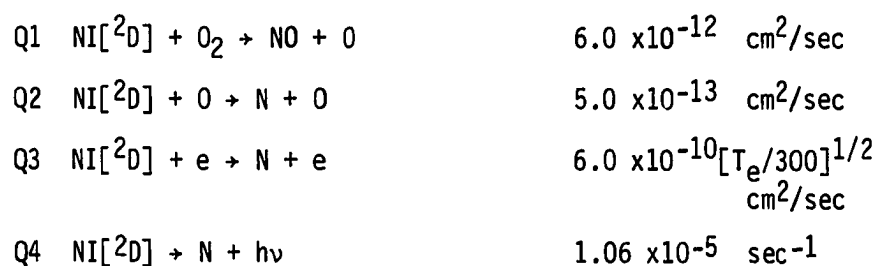
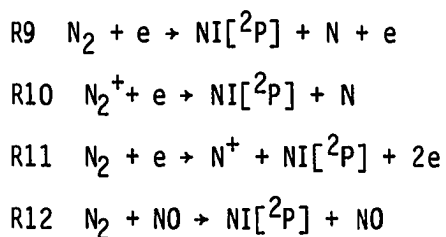


TABLE 4-2

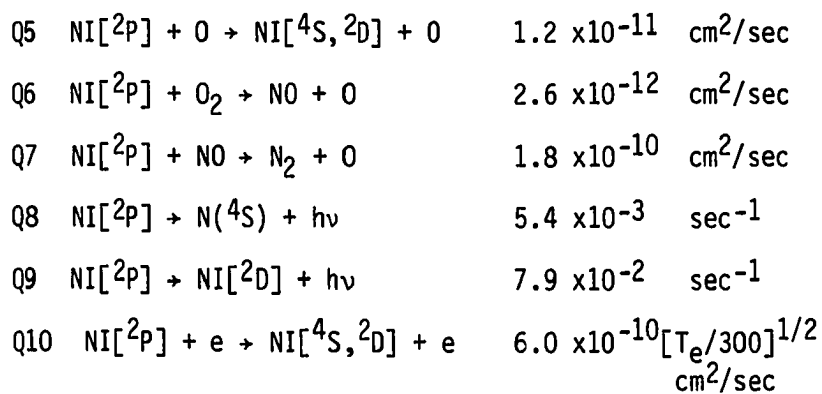
Production and loss mechanisms for the $\text{NI}[^2\text{P}]$ state, which produces the 3466 Å emission.

Production Mechanisms



De-excitation Mechanisms

Rate Constants



Gerard and Harang, 1980). O_2 also contributes significantly to the quenching of the $NI[{}^2P]$ state below 120 km (Zipf et al, 1980).

4.3 Theoretical Considerations

All of the above production and loss mechanisms must be considered in estimating the ratio of $NI[{}^2D]$ to $NI[{}^2P]$ and relating the results to observations i.e. the ratio of $[NI]$ 5200 Å to $[NI]$ 3466 Å. The photon emission rate per unit volume for a species X, undergoing a transition from energy level n to m, may be expressed:

$$J_V(X,n,m) = [X(n)] \times A(n,m) \quad (4-11)$$

where $[X(n)]$ is the concentration of species X in the state n and $A(n,m)$ is the Einstein transition probability for this transition.

The time rate-of-change of the concentration of a state n is:

$$\begin{aligned} \frac{\delta}{\delta t} [X(n)] &= \text{production} - \text{losses} \\ &= J(X,n) - [X(n)] \sum_j A(n,j) - [X(n)] \sum_i Q_i [H_i] \end{aligned} \quad (4-12)$$

where $J(X,n)$ is the production rate of state n, $[X(n)]$ is the concentration of species X in state n, Q_i is the quenching coefficient for species i and H_i is the concentration of the i^{th} quenching species. For a steady state condition, $\frac{\delta}{\delta t} [X(n)] = 0$:

$$[X,n] = J(X,n) / \{ \sum_j A(n,j) + \sum_i Q_i [H_i] \} \quad (4-13)$$

By substituting this result into equation 4-11 we find:

$$J_V(X,n,m) = \frac{A(n,m) \times J(X,n)}{\sum_j A(n,j) + \sum_i Q_i [H_i]} \quad (4-14)$$

We can now determine the emission rate per unit volume of any state n, assuming the related rate coefficients are known.

Including all of the terms for the source and loss equations

listed in Table 4-1 and 4-2 results in an equation similar to 4-14 for each of the emissions. In practice a computer is necessary to effectively handle these equations. By only including the most important reactions, these equations may be simplified for most applications. The important loss reactions for NI[²D] are Q1, Q2 and Q4 so the volume emission rate for the 5200 Å emission may be expressed:

$$J_V(5200) = \frac{1.6 \times 10^{-5} \times J(\text{NI}[\text{}^2\text{D}])}{1.6 \times 10^{-5} + Q_1[\text{O}_2] + Q_2[\text{O}]} \quad (4-15)$$

Where $J(\text{NI}[\text{}^2\text{D}])$ is the total production rate of the [²D] state and Q_1 and Q_2 are the rate constants associated with reactions Q1 and Q2, respectively.

The significant loss reactions for the [²P] state are Q5, Q6, Q8 and Q9 so the volume emission rate is:

$$J_V(3466) = \frac{Q_8 \times J(\text{NI}[\text{}^2\text{P}])}{Q_8 + Q_9 + Q_5[\text{O}] + Q_6[\text{O}_2]} \quad (4-16)$$

Where Q_5 and Q_6 are the quenching coefficients associated with reactions Q5 and Q6, respectively and Q_8 and Q_9 are the Einstein transition probabilities for transitions from the [²P] state. Equation 3-12 depends on the concentrations of all the reactants involved and these concentrations change with altitude. As a result the above equations apply to only a specified altitude so the emission rate must be determined at every altitude in order to produce an altitude profile of the particular emission. This is usually expressed as a graph of altitude versus volume emission rate.

The spectrometers and photometers measure the light emitted by a

column of air extending away from the instrument to infinity. Normally, almost all of the light reaching the instrument is due to scattering or emission by the atmosphere so the column is normally approximated by the height from ground level to the top of the emitting region. The volume emission rate must be integrated along the height of the air column:

$$I = \int_0^{\infty} J_v(\lambda, n, m) dh \quad (4-17)$$

In practice this integration must be performed numerically in the form of a discrete sum by dividing the atmosphere into many thin layers, Δh , and summing over all layers:

$$I = \sum_i J_i(\lambda, n, m) \Delta h \quad (4-18)$$

If all of the important production and loss mechanisms for the emission are accounted for, the light emitted due to a certain excitation can be calculated.

4.4 Model Calculations

Too few experimental studies of the odd nitrogen species have been accomplished to date, leaving many questions unanswered. Attacking these questions by using a theoretical approach, mathematically modeling the aurora, is adding much to our understanding of the odd nitrogen chemistry in auroras.

A significant model calculation involving the entire chemistry of the upper atmosphere was performed by Jones and Rees (Jones and Rees, 1973; Rees and Jones, 1973). This extensive model also included calculations for atomic nitrogen and the production rates of $NI[{}^2D]$ and $NI[{}^2P]$. The major sources of these states were assumed to be

dissociative ionization of N_2 , equation 4-6, dissociative recombination of N_2^+ , equation 4-3, and NO^+ , equation 4-5. Also included was the ion-atom interchange of N_2^+ with O, equation 4-4. None of the relative proportions of the excited atomic nitrogen states were known to Rees and Jones so reasonable values were assumed: equal production of all three states for equations 4-6 and 4-3, 75% of the products formed in $NI[{}^2D]$ for equation 4-5, for equation 4-4, 25% formed in $NI[{}^2D]$ and 75% formed in $NI({}^4S)$. The production of N was related to the production of N_2^+ , yielding production rates:

$$J({}^2P) = .25 \times .33S(N_2^+) + .33 \times 2[N_2^+][e]\alpha_2$$

$$J({}^2D) = .25 \times .33S(N_2^+) + .33 \times 2[N_2^+][e]\alpha_2$$

$$+ .25[N_2^+][O]\gamma_4 + .33 \times 2[N_2^+][e]\alpha_3$$

$$+ 10,400 A ({}^2P + {}^2D)$$

The rate constants used by Rees and Jones were: $\alpha_2 = 2.9 \times 10^{-7} (300/T_e)^{1/3}$, $\alpha_3 = 4.1 \times 10^{-7} (298/T_e)$ and $\gamma_4 = 1.1 \times 10^{-10} \text{ cm}^2/\text{sec}$. The volume emission rates were determined to be:

$$J_V(3466) = \frac{5.4 \times 10^{-3} \times J(NI[{}^2P])}{0.0844 + QR} \text{ cm}^{-3}\text{sec}^{-1}$$

$$J_V(5200) = \frac{1.06 \times 10^{-5} \times J(NI[{}^2D])}{1.06 \times 10^{-5} + QR} \text{ cm}^{-3}\text{sec}^{-1}$$

where the quenching rate was given by:

$$QR = [O_2]\beta_2 + [O_2^+]\gamma_{16} + [NO]\beta_4 \text{ sec}^{-1}$$

Where $\beta_2 = 5.0 \times 10^{-12}$, $\gamma_{16} = 1.8 \times 10^{-10}$ and $\beta_4 = 2.2 \times 10^{-11} \text{ cm}^2/\text{sec}$.

Using the altitude profiles of steady state volume production rates of $[NI]$ 3466 A and $[NI]$ 5200 A calculated by Rees and Jones (1973), the total emission intensity, as viewed from the ground, may be determined by numerically integrating the emission rates at the

various altitudes. Using the altitude profiles calculated by Rees and Jones, the integrated intensities of the 5200 Å and 3466 Å emissions were determined and their ratio was found to be 1.4. This value compares quite favorably with the value of 1.8 ± 0.4 found in this study. However, atomic oxygen was not included as a quenching agent by Rees and Jones (1973), raising some doubt about the validity of the calculations. It has been found that in the midlatitude F-region ionosphere, atomic oxygen is a significant quencher of $\text{NI}[^2\text{D}]$ (Torr et al, 1976). The major quenching species of $\text{NI}[^2\text{P}]$ has since been found to be also atomic oxygen (Golde and Thrusch, 1972; Young and Dunn, 1975; Zipf et al, 1980) for altitudes above 120 km.

A model of odd nitrogen in the thermosphere developed by Oran et al (1975), dealt only with $\text{NI}(^4\text{S})$, $\text{NI}[^2\text{D}]$ and NO . This model also assumes values for the production ratios of $\text{NI}(^4\text{S})$ and $\text{NI}[^2\text{D}]$ and predicts that $\text{NI}[^2\text{D}]$ should be preferentially quenched by O_2 over O . This does appear to be the case below 200 km but is questionable at higher altitudes.

Rees and Roble (1979) developed an auroral substorm model attempting to reproduce anomalous NO concentrations reported earlier (Zipf et al, 1970). The quantity called $\text{NI}[^2\text{D}]$ in this study was actually the sum of both $\text{NI}[^2\text{D}]$ and $\text{NI}[^2\text{P}]$, the two states not being differentiated under the assumption that they act the same in the over-all chemistry. The calculations predict the time varying concentrations of $\text{NI}(^4\text{S})$, $\text{NI}[^2\text{D}]$, and NO during a periodic electron precipitation event. The fractions of $\text{NI}(^4\text{S})$, $[^2\text{D}]$ and $[^2\text{P}]$ produced by

the dissociation of N_2 had not been determined so three cases were considered:

- 1) $1/2 NI[{}^2D] + 1/2 NI({}^4S)$
- 2) $3/4 NI[{}^2D] + 1/4 NI({}^4S)$
- 3) $1/4 NI[{}^2D] + 3/4 NI({}^4S)$

Case 1) predicted a small enhancement of both NO and $NI({}^4S)$. Case 2) predicted a large enhancement of NO at the expense of $NI({}^4S)$ and case 3) predicted just the opposite of case 2). A decrease in the concentration of NO is just the opposite of what had been observed so case 3) seems unlikely and the enhancement of NO in case 1) is not as large as has been observed. Although case 2) seems the most likely, perhaps the actual value lies somewhere between cases 1) and 2). The fractions determined by Zipf et al (1980), for the dissociative ionization of N_2 correspond to a value somewhere between cases 1) and 2), indicating that this is a strong possibility.

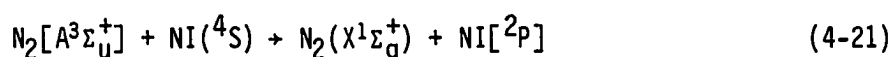
According to the previous studies, already cited, the most important reaction for the production of $NI[{}^2P]$ in the aurora is believed to be the dissociation of N_2 (reaction R9) by electron impact. This reaction is also a major source of $NI[{}^2D]$ and since this state is also produced by the $NI[{}^2P \rightarrow {}^2D]$ transition (cascading) it would be reasonable to assume that more $NI[{}^2D]$ than $NI[{}^2P]$ should be produced. While the dissociation of N_2 is thought to produce a large percentage (80-90%) of $NI[{}^2P]$ atoms, it contributes only about a third of the $NI[{}^2D]$ atoms. The dissociative recombination of NO^+ (reaction R5) is believed to contribute about one-third of the $NI[{}^2D]$ atoms in the

aurora and the ion-atom interchange of N_2^+ with O (reaction R3) is thought to provide almost as many. The production mechanisms for $NI[{}^2D]$ appear to have very high efficiencies; 80% or better for reactions R1, R2 and R5 with reaction R3 thought to be almost 100% efficient (Rusch and Gerard, 1980; Oran et al, 1975).

Laboratory studies indicate a larger cross section for the ionization of N_2 than dissociation by electron impact. The dissociation of N_2 produces NI in both the $[{}^2D]$ and $[{}^2P]$ states through reactions R1, R2, R9 and R11 while the ionization of N_2 produces only the $[{}^2D]$ state, through reactions R3 and R4 and studies of these two reactions indicate a large reaction rate. Consequently with more sources for $NI[{}^2D]$ than $NI[{}^2P]$ it would be expected that significantly more $NI[{}^2D]$ than $NI[{}^2P]$ would be produced in the aurora. A recent theoretical calculation of the 5200 Å to 3466 Å ratio by Rees (private communication, 1981) predicts a value of about 30 while the measurements of this study show a value of 1.8 ± 0.4 . The current measurements therefore indicate, either a much smaller population of $NI[{}^2D]$ than implied by the sources given in Table 4-1 or a larger population of $NI[{}^2P]$ than suggested by the sources listed in Table 4-2.

The relatively large discrepancy between the measurements and the most recent model predictions may be reconciled in two ways. First, the $NI[{}^2D]$ yield from reaction R4 cannot be measured directly because of the severe quenching effects of $NI[{}^2D]$. It is possible that this reaction is not as efficient as is currently assumed, and consequently the model calculations over-estimate the $NI[{}^2D]$ popula-

tion. Alternatively, if the accepted rates for the sources of NI[²D] are correct then additional sources of NI[²P] must be sought. A possible source of the NI[²P] state that has not been considered in any model calculations reported in the literature is the interaction of N₂[A³Σ_u⁺] with NI(⁴S):



An analogous process between N₂[A³Σ_u⁺] and OI(³P) has been suggested to account for the auroral OI[²S + ³P] 5577 Å emission. It is plausible that reaction 4-21 may be equally efficient in producing NI[²P].

Another possibility is the reaction of vibrationally excited N₂⁺ with O to produce NO⁺ and NI[²P] as suggested by Zipf et al (1980):



Such reactions may explain why the 5200 Å measurement of Rusch and Gerard (1980) required such high efficiencies for the sources of NI[²D] to be reconciled, through cascading from a larger than expected NI[²P] population.

In conclusion, the most important result of the research for this thesis project is to force a re-evaluation of the present understanding of the sources for NI[²D] and NI[²P] in high latitude, particle precipitation events.

CHAPTER 5

SUMMARY

The $\text{NI}[^2\text{D}]$ and $\text{NI}[^2\text{P}]$ excited electronic states of atomic nitrogen are created by electron impact in the aurora. This occurs through three major processes; 1) the dissociation of N_2 producing both excited states directly, 2) the dissociative ionization of N_2 , which may produce both excited states directly and indirectly and 3) the ionization of N_2 which generates both states indirectly through reactions involving N_2^+ . Once produced, most of the atoms in the excited states are quenched by atomic and molecular oxygen. The NI atoms in the $[^2\text{D}]$ and $[^2\text{P}]$ states left unquenched relax radiatively, emitting 5200 Å and 3466 Å photons. The absolute intensities of the emissions are functions of the populations of the excited states producing them. By simultaneously measuring these intensities, relations between the excited states, and the ground state, can be inferred. Again it should be stressed that the measurements of the 3466 Å and 5200 Å emissions in this study were not only taken at the same time but also from the same region of the auroral display.

Extensive simultaneous spectroscopic measurements of the auroral $\text{NI}[^2\text{D} \rightarrow ^4\text{S}]$ 5200 Å and $\text{NI}[^2\text{P} \rightarrow ^4\text{S}]$ 3466 Å emissions show that the ratio of these two emissions is 1.84 ± 0.40 in the aurora. Within the accuracy of the measurements reported here ($\pm 22\%$), this ratio is independent of the energy of the auroral particles precipitating into the atmosphere. The best fitting straight line of Figure 3.2 passes

through the origin (within the experimental error) as would be expected, assuming electron impact is the major excitation source. The electron energy spectrum in the aurora is broad enough that any precipitation producing NI[²D] should also produce NI[²P], through the reactions in Chapter 4. A comparison between Figures 3.1 and 3.2 illustrates that the 5200 Å to 3466 Å intensity ratio is very sensitive to cloud cover.

The values of the 5200 Å to 3466 Å ratio derived from auroral models are quite diverse. The value of 1.45 determined from the model by Rees and Jones (1973) is comparable to the present findings, but this model did not include atomic oxygen as a quenching agent. A more recent calculation by Rees predicts a ratio of approximately 30. A value comparable with the value observed in the present study could possibly be arrived at if reaction R3 (Table 4.1) is not actually as efficient as has been assumed at producing NI[²D] or if another excitation mechanism for NI[²P] exists and has not been taken into account in the models. In comparing the present experimental result with the current model calculations it becomes obvious that there are definite discrepancies which must be addressed. Our understanding of the auroral processes must be re-evaluated as far as the chemistry of atomic nitrogen is concerned and this could be greatly facilitated if more studies involving the excited states of atomic nitrogen were undertaken. Although progress is being made, there is still much to accomplish before an understanding of the odd nitrogen species and their processes in the aurora is achieved.

APPENDIX
ERROR CALCULATIONS

The accuracy of the various measured quantities referred to in the text were determined using standard procedures for the determination of non-systematic error (Beers, Y., 1953).

For a quantity t , with an associated variation of Δt , the range of error associated with the measurement (in percent) is:

$$R = \frac{\Delta t}{t} \times 100$$

So the quantity and its associated error is; $t \pm R/2 \%$.

A sample calculation of the accuracy of the calibration factor for the 5200 Å emission is as follows:

- 1) The distance d (see Figure A.1) enters the calculation in equation 3-4 as d^2 . Since $d=20.75 \pm 0.10$ meters, $\Delta d=0.20$ m.

$$DS = \frac{2\Delta d}{d} \times 100 = \frac{0.4}{20.75} \times 100 = 1.93\% \approx \pm 0.96\%$$

- 2) The angle $\delta=25 \pm 5^\circ$ and enters the calculation as $\cos\delta$ so:

$$SC = \frac{\Delta \cos\delta}{\cos\delta} \times 100 = \frac{\cos 20 - \cos 30}{\cos 25} \times 100 = 8.1\% \approx \pm 4.1\%$$

- 3) For $c=4350$ counts, the photon statistics shows $\Delta C=2(4350)^{1/2}$ so:

$$CT = \frac{\Delta C}{C} \times 100 = \frac{2(4350)^{1/2}}{4350} \times 100 = 3.0\% \approx \pm 1.5\%$$

- 4) The halfwidth measurement was $\lambda=5.85 \pm .20$ Å so $\Delta\lambda=.40$ and:

$$HE = \frac{\Delta\lambda}{\lambda} \times 100 = \frac{0.40}{5.85} \times 100 = 6.8\% \approx \pm 3.4\%$$

All the terms above are combined as products along with the accuracy of the calibration lamp measurement (I_c) and the correction factor for atmospheric extinction (CF) to form the calibration factor. The total accuracy of the calibration factor can be determined by

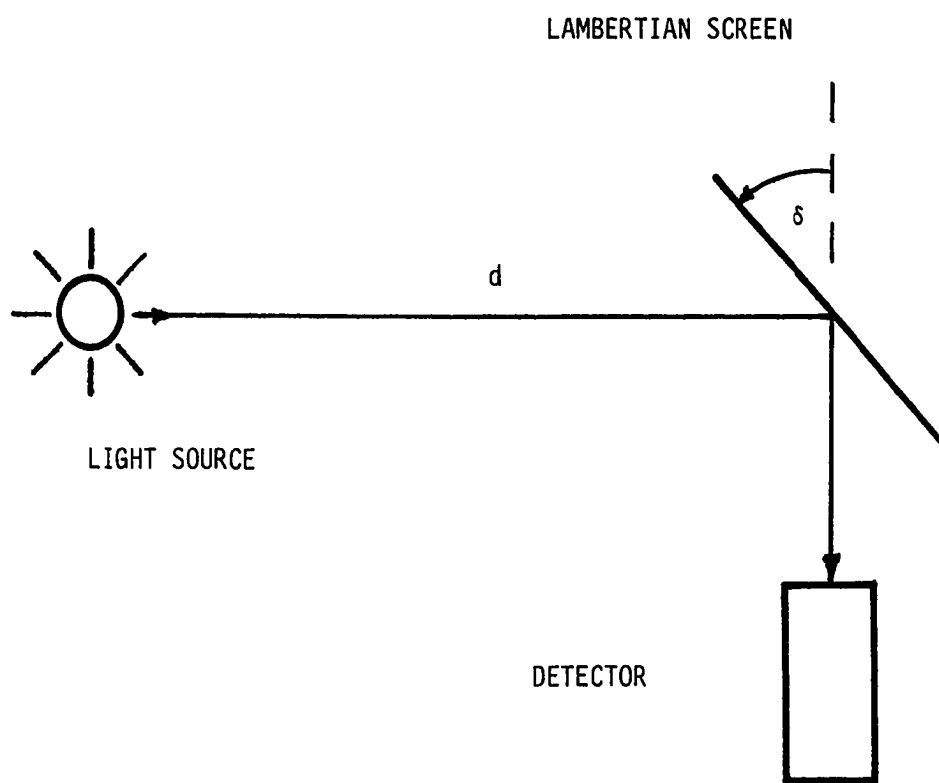


Figure A.1 The setup for the absolute intensity calibrations.

observing how the errors are propagated through the calculation.

This propagation can be shown to be:

$$TE = \{(DS)^2+(SC)^2+(CT)^2+(HE)^2+(Ic)^2+(CF)^2\}^{1/2}$$

So the total error (TE) in the 5200 A calibration factor calculation can be found to be:

$$\begin{aligned} TE(5200 \text{ A}) &= \{(1.93)^2+(8.1)^2+(3.0)^2+(6.8)^2+(10)^2+(30)^2\}^{1/2} \\ &= 33.5\% \approx \pm 17\% \end{aligned}$$

Hence a calibration factor of 1.5 ± 0.3 R/count.

BIBLIOGRAPHY

- *Beers, Y., Introduction to the Theory of Error, Addison-Wesley Publishing, Cambridge, 1953.
- Borst, W.L. and Zipf, E.C., Cross Section for Electron-Impact Excitation of the (0,0) First Negative Band of N₂ from Threshold to 3 KeV, Phys. Rev. A, 1, 834, 1970.
- Chamberlain, J.W., Physics of the Aurora and Airglow, Academic Press, New York, 1961.
- *Courtes, G., La raie ⁴S-²D de l'azote observ'ee au cr'epuscule, Comp. Rend. Acad. Sci. Paris, 231, 62, 1950.
- *Davis, T.N., Hallinan, T.J., Mead, G.D., Mead, J.M., Trichel, M.C. and Hess, W.N., Artificial Aurora Experiment: Ground-Based Optical Observations, J. Geophys. Res., 76, 6082, 1971.
- *Davis, T.N., Hess, W.N., Trichel, M.C., Wescott, E.M., Hallinan, T.J., StenBack-Nielsen, H.C. and Maier, E.J.R., Artificial Aurora Conjugate to a Rocket-Borne Electron Accelerator, J. Geophys. Rev., 85, 1722, 1980.
- *Deehr, C.S., Sivjee, G.G., Egeland, A., Henriksen, K., Sandholt, P.E., Smith, R., Sweeney, P., Duncan, C., and Gilmer, J., Ground-Based Observations of F Region Aurora Associated With the Magnetospheric Cusp, J. Geophys. Rev., 85, 2185, 1980.
- *Donahue, T.M., Positive Ion Chemistry of the D and F region, Radio Sci., 7, 73, 1974.
- Engebretson, M.J., Mauersberger, K., Kayser, D.C., Potter, W.E. and Nier, A.O., Empirical Model of Atomic Nitrogen in the Upper Thermosphere, J. Geophys. Rev., 82, 461, 1977.
- Engebretson, M.J., DeFreese, J.A. and Mauersberger, K., Diurnal, Seasonal and Night-time Variations of Atomic Nitrogen in the Equatorial Thermosphere, J. Geophys. Rev., 85, 2165, 1980.
- *Fastie, W.G., Image Forming Properties of the Ebert Monochromator, J. Opt. Soc. Am., 42, 647, 1952.
- *Frederick, J.E., and Rusch, D.W., On the Chemistry of Metastable Atomic Nitrogen in the F Region Deduced from Simultaneous Measure-

References preceded by "*" have been cited in the text.

- ments of the 5200 Å Airglow and Atmospheric Composition, J. Geophys. Res., 82, 3509, 1977.
- *Garstang, R.H., Multiplet Intensities for the Lines $4S-2D$ of OI, OII and NI, Astrophys. J., 115, 506, 1952.
- *Garstang, R.H., "The Airglow and the Aurorae", Pergamon, London, 1956.
- *Gerard, J.C. and Harang, O.E., Metastable $N(2P)$ Atoms in the Aurora, J. Geophys. Res., 85, 1757, 1980
- *Handbook of Geophysics and Space Environments, AFCRL, 1965.
- *Hess, W.N., Trichel, M.C., Davis, T.N., Beggs, W.C., Kraft, G.E., Stassinopoulos, E. and Maier, E.J.R., Artificial Aurora Experiment: Experiment and Principal Results, J. Geophys. Res., 76, 6067, 1971.
- Hyman, E., Strickland, D.J., Julienne, P.S., and Strobel, D.F., Auroral NO Concentrations?, J. Geophys. Res., 81, 4765, 1976. 1971.
- *Hyman, E., Strickland, D.J., Julienne, P.S., and Strobel, D.F., Auroral NO Concentrations?, J. Geophys. Res., 81, 4765, 1976.
- *Jones, R.A. and Rees, M.H., Time Dependant Studies of the Aurora -I. Ion Density and Composition, Planet. Space Sci., 21, 537, 1973.
- *Kaplan, J., High-pressure Afterglow in Nitrogen, 645; A New Nitrogen Line, Nature, 141, 1139, 1938.
- Kohnlein, W., Kramkowsky, D., Lammerzahn, P., Joos, W. and Volland, H., A Thermospheric Model of the Annual Variations of He, N, O, N_2 and Ar from the Aeros Nims Data, J. Geophys. Res., 84, 4355, 1979.
- *Narcisi, R.S., Bailey, A.D., Thomas, D.M., and Wlodyka, L.E., D and F Region Positive Ion Composition During and Auroral Absorption Event (abstract), EOS Trans. AGU, 55, 376, 1974.
- *Oran, E.S., Julienne, P.S. and Strobel, D.F., The Aeronomy of Odd Nitrogen in the Thermosphere, J. Geophys. Res., 80, 3068, 1975.
- *Pasternack, S., Transition Probabilities of Forbidden Lines, Astrophys. J., 92, 129, 1940.
- *Rees, M.H. and Jones, R.A., Time Dependent Studies of the Aurora-II. Spectroscopic Morphology, Planet. Space Sci., 21, 1213, 1973.
- *Rees, M.H. and Luckey, D., Auroral Electron Energy Derived from Ratio of Spectroscopic Emissions 1. Model Computations, J. Geophys. Res., 79, 5181, 1974.

- *Rees, M.H., Magnetospheric Substorm Energy Dissipation in the Atmosphere, *Planet. Space Sci.*, 23, 1589, 1975.
- *Rees, M.H. and Roble, R.G., The Morphology of N and NO in Auroral Substorms, *Planet. Space Sci.*, 27, 453, 1979.
- *Rusch, D.W. and Gerard, G-C., Satellite Studies of N(²D) Emission and Ion Chemistry in Aurorae, *J. Geophys. Res.*, 85, 1285, 1980.
- *Sivjee, G.G., Deehr, C.S. and Henriksen, K., Difference in Quenching of N(²D_{3/2}) and N(²D_{5/2}) by Atomic Oxygen, *J. Geophys. Res.*, 86, 1581, 1981.
- *Slanger, J.G., Wood, B.J., and Black, G., Temperature Coefficients for N(²D) Quenching by O₂ and N₂O, *J. Geophys. Res.*, 76, 8430, 1971.
- *Slipher, V.M., and Sommer, L.A., Deutung des Nordlichtspektrums, *Naturwissenschaften*, 17, 802, 1929.
- *Torr, M.R., Burnside, R.G., Hays, P.B., Stewart, A.I., Torr, D.G. and Walker, J.C.G., Metastable ²D Atomic Nitrogen in the Mid-Latitude Nocturnal Ionosphere, *J. Geophys. Res.*, 81, 531, 1976.
- Vallance Jones, A., *Aurora*, Geophysics and Astrophysics Monographs, D. Reidel Publishing Co., V9, 1974.
- *Vallance Jones, A., and Gattinger, R.L., Quantitative Spectroscopy of the Aurora, III, The Spectrum of Medium Intensity Aurora Between 3100 Å and 4700 Å, *Can. J. Phys.*, 53, 1806, 1975.
- *Young, R.A., and Dunn, O.J., The Excitation and Quenching of N(²P), *J. Chem. Phys.*, 63, 1806, 1975.
- *Zipf, E.C., Borst, W.L., and Donahue, T.M., A Mass Spectrometer Observation of NO in and Auroral Arc, *J. Geophys. Res.*, 75, 6371, 1970.
- Zipf, E.C. and McLaughlin, R.W., On the Dissociation of Nitrogen by Electron Impact and by E.U.V. Photo-Absorption, *Planet. Space Sci.*, 26, 449, 1978.
- *Zipf, E.C., Espy, P.J. and Boyle, C.F., The Excitation and Collisional Deactivation of Metastable N(²P) Atoms in Auroras, *J. Geophys. Res.*, 85, 687, 1980.
- Zipf, E.C. and Wells, W.C., Emission Line Shapes Produced by Dissociative Excitation of Atmospheric Gases, *Planet. Space Sci.*, 28, 859, 1980.